



Review

Recent advances in sensing the inter-biomolecular interactions at the nanoscale – A comprehensive review of AFM-based force spectroscopy

Anabel Lostao^{a,b,c,*}, KeeSiang Lim^d, María Carmen Pallarés^{a,b}, Arkadiusz Ptak^e, Carlos Marcuello^{a,b,*}^a Instituto de Nanociencia y Materiales de Aragón (INMA), CSIC-Universidad de Zaragoza, Zaragoza 50009, Spain^b Laboratorio de Microscopías Avanzadas (LMA), Universidad de Zaragoza, Zaragoza 50018, Spain^c Fundación ARAID, Aragón, Spain^d WPI-Nano Life Science Institute, Kanazawa University, Ishikawa 920-1192, Japan^e Institute of Physics, Faculty of Materials Engineering and Technical Physics, Poznan University of Technology, Poznan 60-925, Poland

ARTICLE INFO

Keywords:

Atomic force microscopy
Force spectroscopy
Bioconjugation and surface modification
High-speed AFM
Molecular recognition imaging
Single molecule interactions

ABSTRACT

Biomolecular interactions underpin most processes inside the cell. Hence, a precise and quantitative understanding of molecular association and dissociation events is crucial, not only from a fundamental perspective, but also for the rational design of biomolecular platforms for state-of-the-art biomedical and industrial applications. In this context, atomic force microscopy (AFM) appears as an invaluable experimental technique, allowing the measurement of the mechanical strength of biomolecular complexes to provide a quantitative characterization of their interaction properties from a single molecule perspective. In the present review, the most recent methodological advances in this field are presented with special focus on bioconjugation, immobilization and AFM tip functionalization, dynamic force spectroscopy measurements, molecular recognition imaging and theoretical modeling. We expect this work to significantly aid in grasping the principles of AFM-based force spectroscopy (AFM-FS) technique and provide the necessary tools to acquaint the type of data that can be achieved from this type of experiments. Furthermore, a critical assessment is done with other nanotechnology techniques to better visualize the future prospects of AFM-FS.

1. Introduction

Adhesion forces are ubiquitous in nature. For this reason, understanding how biomolecular complexes form and dissociate is a problem of intrinsic interest in biological sciences. The constituent entities which conform life are sugars [1], lipids [2], proteins [3] and nucleic acids, namely deoxyribonucleic/ribonucleic acids (DNA and RNA, respectively) [4,5]. Carbohydrate-carbohydrate and carbohydrate-protein interactions provide the functional attributes to food [6]. Due to this, food industry invests large amounts of funds to discern the above described biomolecular binding. Moreover, protein glycosylation is a post-translational modification (PTM) that accounts for the addition of glycans to proteins which impacts on their adhesion properties. Glycans play a pivotal role to control the protein folding inside eukaryotic cells [7]. PTM pathways in the biochemical pathogenesis affects cell-cell recognition [8] which could lead a panoply of human diseases like postnatal hearing loss [9], congenital muscular dystrophy [10] or

cobblestone lissencephaly [11], among many others. The formation of lipid layers is of fundamental interest because their fluidity and polarity directly depends on how lipid chains are associated with membrane proteins and other lipids. Self-assembly properties of lipids to create lamellar organized systems enable the integration of these biomimetic membrane proteins for fundamental research. Industrial applications related to lipid membranes have been developed, such as the production of tailored transistor devices by integrating ion channels into gold nanowires [12]. Other illustrative example is the case of liposomal systems typically employed for nano-encapsulation of bioactive molecules for drug delivery treatments [13]. Then, the proper protein interactions inside cells underlie many scaffolds typically found for their homeostasis and organism survival. For instance, extracellular signal-regulated kinase (ERK) cascade is a signaling pathway for cell differentiation and proliferation [14]. Proteins are also targets for innovative industrial applications. Screen-printed chemiluminescence protein biochips for simultaneous monitoring of several point-of-care biomolecules

* Corresponding authors at: Instituto de Nanociencia y Materiales de Aragón (INMA), CSIC-Universidad de Zaragoza, Zaragoza 50009, Spain.

E-mail addresses: aglostao@unizar.es (A. Lostao), cmarcuel@unizar.es (C. Marcuello).<https://doi.org/10.1016/j.ijbiomac.2023.124089>

Received 8 February 2023; Received in revised form 13 March 2023; Accepted 15 March 2023

Available online 21 March 2023

0141-8130/© 2023 The Author(s). Published by Elsevier B.V. This is an open access article under the CC BY-NC-ND license (<http://creativecommons.org/licenses/by-nc-nd/4.0/>).

[15] or the design of next-generation of bioelectronic sensors based on redox proteins [16] evidence the promising perspectives in the use of proteins in technology markets. Furthermore, bioreactors coated with recombinant proteins can be manufactured to obtain high-value products as therapeutic compounds [17]. Finally, the technology associated with nucleic acids is prolific. DNA microarrays consist of a solid-surface collection of exposed DNA strands that can be hybridized with other nucleic acid strands to evaluate the gene expression profiling levels [18], genotype multiple regions of the animal genome [19], or identify transcription factor binding locations linked to cell aging [20] which is one of the main fingerprints to succeed in the prognosis of malignancies [21]. Catalytic RNA sequences, also known as ribozymes [22], have been extensively engineered for genetic devices related to synthetic biology [23] or programmable sensor devices to detect a multitude of other biomolecules of trace metal concentrations [24,25]. These aspects underline the need to find out the mechanisms of how these biomolecules interact with each other. To understand the molecular underpinnings of living systems, classical bulk techniques like surface plasmon resonance (SPR) [26], fluorescence cross-correlation spectroscopy (FCCS) [27], radiolabeling [28] or bioluminescence resonance energy transfer (BRET) [29] are typically employed. The main limitations of these approaches are the loss of data attributed to individual entities as the identification of molecular sub-populations, short-lived states, and rare molecular events [30] due to the ensemble averaging intrinsic to bulk techniques. To overcome the aforementioned constraints, single molecule techniques have been developed. For bigger entities like bacteria and cells, there exists a broader range of force spectroscopy approaches like micropipette assays [31], reflection interference contrast microscopy (RICM) [32], and biomembrane force probe (BFP) [33] to measure cellular adhesion forces. In contrast, the number of available tools to decipher intra- or intermolecular interactions between small biomolecules is more limited. Here, we can find single molecule fluorescence resonance energy transfer (SM-FRET) [34,35] and nanoscience tools capable to measure the tiny forces involved at the single molecule level. In the last group we find optical tweezers (OT), based on a laser beam which provides attractive/repulsive forces to physically hold and move typically one or two dielectric microbeads where biomolecules are attached on their respective ends [36]. It has been also reported cases where one end of the molecule was bound to the trapped bead while the other end remained immobilized on a solid surface [37]. This latest example is relevant to assess intramolecular interactions like the existing on viral DNA loops where one of its ends is attached on the bead, whereas the other biotinylated extreme interacts with a streptavidin coated solid surface [38]. Thus, OT can stretch biomolecules by moving one of the beads to which it is attached, allowing the measurement of adhesion forces. Typically, OT has been successfully employed to determine intramolecular interactions like the unfolding of multidomain proteins [39], like the von Willebrand factor [40], or the stretching of DNA [41] and RNA [42] nucleic acids. Recently, it has been reported several works where OT addresses the intermolecular interactions involved between two biomolecules of different nature like the binding of glycoproteins and small protein domains [43], dendrimer ligands on telomeric G-quadruplex DNA [44], the strength of DNA conformation on microtubule composites [45], the interaction of DNA with DNA alkyltransferase enzyme [46], the stabilization of transfer RNA with 30S ribosomal subunits [47], and the transcriptional processes among RNA polymerase and supercoiled DNA under torsion [48]. It is remarkable to point out that OT can be combined with FRET measurements to gather simultaneously the binding strength and data on the molecular dynamics, respectively [49]. In the piconewton range measuring tools we can also find the magnetic tweezers (MT) that use magnetic microbeads which can be manipulated by external magnetic fields [50]. In the case of MT, the position of these microbeads is monitored in three dimensions by an inverted optical microscope integrated with a charge coupled device (CCD) or complementary metal oxide semiconductor (CMOS) cameras. MT has shown to

be one of the best techniques to manipulate ultra-low forces (<20 pN), being able to operate in constant force mode. MT offers unparalleled simplicity and versatility in the design of downstream applications for biological systems [51]. MT has achieved unprecedented force resolution in the study of intramolecular forces of titin protein [52] or protein L [53] and intermolecular interactions of unzipping DNA strands [54], vinculin: talin focal adhesion proteins [55], and DNA:protein complexes [56], among others. The main disadvantage of OT and MT is the lack of capability to conduct topography or force mapping, to which it must be added that there are still no commercial MT systems. The last nanotechnology tool capable to detect ultralow forces at the nanoscale is the atomic force microscope (AFM). AFM emerged as a powerful tool to address the physicochemical properties of soft matter at the nanometric scale since its discovery in 1986 [57]. The working principle of AFM is based on a flexible micro (canti)lever that approaches the sample surface with a sharp tip. The cantilever tip-sample interaction is followed through the deflection of the cantilever monitored by a laser beam reflected off the back-side of the lever. The sample is attached typically on a substrate mounted on a piezoelectric actuator—in other systems is the lever that moves attached to the scanner—, capable to control its three-dimensional motions with angstrom accuracy as a response to the applied voltages. The beam is detected by a quadrant photodiode which measures the normal and torsional signals of the lever [58], while the voltage is recorded by the digital signal processing (DSP) electronic board, which provides a response depending on the feedback close-loop of the system [59]. AFM exhibits advantages over other techniques, including the ability to conduct experiments in aqueous media, mimicking intracellular conditions [60,61]. The structure and function of biological entities are highly dependent on their hydration state. For this reason, operating AFM in fluid allows studying the behavior of a broad range of biological systems in relevant conditions by addressing the topology of individual molecules or particles and also their association patterns giving insights on the interactions involved between individual biomolecules with unprecedented spatial and temporal resolution.

Moreover, AFM does not require the labelling or coating of the samples with contrast agents like other techniques do, such as FRET [35,62] or scanning electron microscopy (SEM) [63], respectively. Similarly, techniques such as immunocytochemistry approaches, SEM, and transmission electron microscopy (TEM) commonly require sample fixation with formaldehyde or glutaraldehyde agents [64], but these compounds are dangerous for human health and may induce chemical changes in the samples, losing their functionality. AFM circumvents these drawbacks and only requires the physical immobilization of the sample, as imaging entails scanning of the sample with the tip to obtain the topography and other property maps depending on the operational mode used [65]. The continuous development of technical improvements and different operational modes has turned AFM into a multi-parametric imaging toolbox providing maps on multitude of properties of the sample [66]. Nowadays, there exist commercially available AFM tips with a curvature final radius below 2 nm, which minimizes the non-desirable broadening effects during image acquisition [67]. AFM imaging was successfully employed to probe from carbohydrates conformation [68], the integrity of lipid layers [69], the enzymatic oligomerization induced by ligand binding and catalysis [70–73], self-assembly of small peptides [74], the flexibility of the loops involved in glycosyltransferases catalysis [75], to resolve the DNA helix structure [76] and the A-form sub-helical pitch periodicity of dsRNA double helices [77]. Finally, AFM imaging has also been used to carry out experiments with biomolecules of different nature, like lipid domains with bovine intestinal alkaline phosphatase (BIAP) protein [78] or ferric uptake regulators (Fur) with DNA promoters [79,80]. Remarkably, there are other available modes less used but with great potential. Then, high-speed AFM (HS-AFM) is based on increasing the imaging rates by driving up the resonant frequencies of cantilevers with low spring constants by reducing the lever dimensions [81]. Currently, HS-AFM is mainly

applied to scan biomolecular transition or biomolecular interaction in fluid with high spatiotemporal resolution, in which it may be impossible for other techniques such as X-ray crystallography, cryoEM, and optical microscopy. For example, the application of HS-AFM on dynamic viral proteins such as fusion proteins [82–84] and capsid proteins [85] is useful to face devastating infectious diseases. The high scanning rate of HS-AFM is favorable for the characterization of the conformational properties of intrinsically disordered proteins (IDPs) [86]. Up to date, structural details of many IDPs remain poorly resolved using Cryo-EM. The advancement in computational biology has included deep-learning software tools for protein structure prediction. These tools include AlphaFold 2 [87] and RoseTTAFold [88] that can predict the 3D structure of proteins based on amino acid sequences with high accuracy. A combination of deep-learning algorithms and HS-AFM could produce promising research outputs, particularly for IDPs. Interaction between the intrinsically disordered regions (IDRs) of IDPs is prerequisite for liquid-liquid phase separation (LLPS). HS-AFM provides a nanoscopic platform to investigate the regulator factors of LLPS [89]. Besides biomolecules, HS-AFM is applicable to elucidate the structural and functional properties of organelles. The real-time dynamic activity of intrinsically disordered FG filaments in nuclear pore complex (NPC), which regulates nucleocytoplasmic trafficking, can be measured using HS-AFM [90,91]. Extracellular organelles, exosomes for example, have been used as the docking sites for viral fusion proteins to study their entry mechanisms through HS-AFM imaging [82,84]. The near physiological scanning environment provided by HS-AFM system is also suitable for living cells such as bacteria [92,93] and mammalian cells [94], or lipid layer dynamics in the presence of amyloidogenic proteins [95]. Technical improvement of HS-AFM is essential to enhance its capabilities. The nanoscale infrared AFM (AFM-nanoIR) technique is customized with a second IR pulsed tunable beam focused on the same region of the scanned sample by the classical AFM tip. This fact results in a photothermal expansion of the absorbing regions of the sample, inducing a cantilever oscillation proportional to the aforementioned IR absorption [96]. AFM-nanoIR provides direct correlation of topography images from local sample areas with chemical mapping. The location of protein receptors on carcinogenic cells [97] and the interactions of amyloidogenic proteins with lipid layers [98] or small molecule inhibitors [95] have been addressed by this technique. The monitoring of chemical reactions that take place between biomolecules is expected to be covered by AFM-nanoIR. AFM imaging is introduced for the reason that this operational mode is the most widely exploited which is available in all AFM setups, whereas AFM-nanoIR fine-contribute to grasp the surface chemical properties of the tested samples which is complementary respect to the topic of the present review. Other available operational modes to elicit physico-chemical properties of biomolecules, living cells or other type of nanomaterials are the following: AFM scanning electrochemical microscopy (AFM-SECM) [99], conductive AFM (C-AFM) [100], kelvin probe force microscopy (KPFM) [101], magnetic force microscopy (MFM) [102] and nanoindentation by AFM [103], where the faradaic current reactivity, electrical current transmission, sample surface potential, magnetic response and nanomechanical properties (elastic modulus, viscoelasticity, dissipation, ...) are assessed, respectively.

Finally, force spectroscopy by AFM (AFM-FS) allows probing, as optical and magnetic tweezers, biomolecular adhesion forces at the single molecule level [104]. AFM-FS measurements with biological entities are carried out in liquid media, mimicking nature, removing the unspecific capillarity tip-sample forces observed in air conditions [105]. AFM-FS can obtain information related to the intramolecular interactions of proteins and DNA/RNA strands by pulling or stretching one molecule, a fragment or a multidomain protein [106,107]. In the case of proteins, in addition to observing phenomena hidden in unfolding bulk measurements, force is the main unfolding agent *in vivo*. Furthermore, AFM-FS analyzes the molecular interactions of two single biomolecules attached on substrate surface and AFM tip like the displayed between

single stranded DNA-protein [108] and RNA-protein [109], respectively, or on cellular membranes, having these experiments experienced great advances in the last years. Pioneering AFM-FS experiments using flexible tethers to covalently attach molecules on AFM tips date in the 1990s focusing on ligand unbinding in (strept)avidin:biotin [110] and antibody:antigen [111] systems, due to their displayed strong interactions. First, (strept)avidin:biotin presents one of the strongest non-covalent complex known in biology. Then, the large number of hydrogen bonding established between epitope regions from antigens and the respective antibodies also render strong interactions. The continuous optimization, design, and development of AFM setups in parallel with softer AFM probes has allowed measuring lower rupture forces from transient biomolecular complexes. This work will discuss in detail these topics in the following sections: i) AFM-FS working principles, ii) functionalization strategies to develop AFM-FS, iii) analysis and interpretation of AFM-FS experiments, iv) molecular recognition imaging, v) limitations of AFM and alternatives, and vi) conclusions and future perspectives. We expect that the present manuscript will contribute to better understand AFM-FS principles; serve as a groundwork to keep attention of the potentialities of AFM-FS to study biological systems; prevent flaws during the devise of AFM-FS experiments and properly interpret the obtained data in order to minimize data scattering.

2. AFM-FS working principles

An AFM setup is integrated with multiple components where the cantilever is the most important one (Fig. 1). The cantilever works as a force probe that allows sensing adhesions with a sample with high resolution by measuring its deflection in real-time. Thus, the interactions between the sample and the end of the cantilever, which can be bare or carry a molecule linked onto the tip through covalent procedures, can be sensed and analyzed. The force that senses the cantilever is expressed in the linear-Hookean force relationship (Eq. (1)) [112]:

$$F = -k\Delta x \quad (1)$$

where F is the force measured, k is the spring constant of the cantilever, and Δx is the deflection of the cantilever (Fig. 1). By measuring the cantilever deflection, the force that involves the AFM probe is inferred. Soft cantilevers with low spring constants exhibit greater sensitivity. For this purpose, the cantilever dimensions should be thin and long. Nevertheless, extremely high cantilever bending can generate greater instabilities during data acquisition in addition to the loss of force-range measurements [113]. For this reason, the choice of the cantilever probe is not trivial and must take into account the force range expected to be measured. The cantilever works as a harmonic oscillator when it is free of sensing external forces described thus, by its natural frequency (w_0 , Eq. (2)) and quality factor (Q factor, Eq. (3)):

$$w_0 = \sqrt{\frac{k}{m}} \quad (2)$$

$$Q = \sqrt{\frac{m k}{\gamma}} \quad (3)$$

where terms m and γ are the effective AFM cantilever mass and its damping coefficient, respectively. Q factor is the ratio established between the energy stored to the energy lost in one radian of an oscillation cycle. For this reason, the Q factor is another key aspect to be considered in dynamic measurements [114]. Since AFM-FS works in static regime the Q factor is not a relevant aspect to contemplate. It is the opposite scenario for those molecular recognition studies based on the phase shift during the image acquisition. Lower Q factor values indicate that the cantilever oscillator loses a large amount of energy during its vibration. Lower Q factor values have a positive contribution for AFM-FS

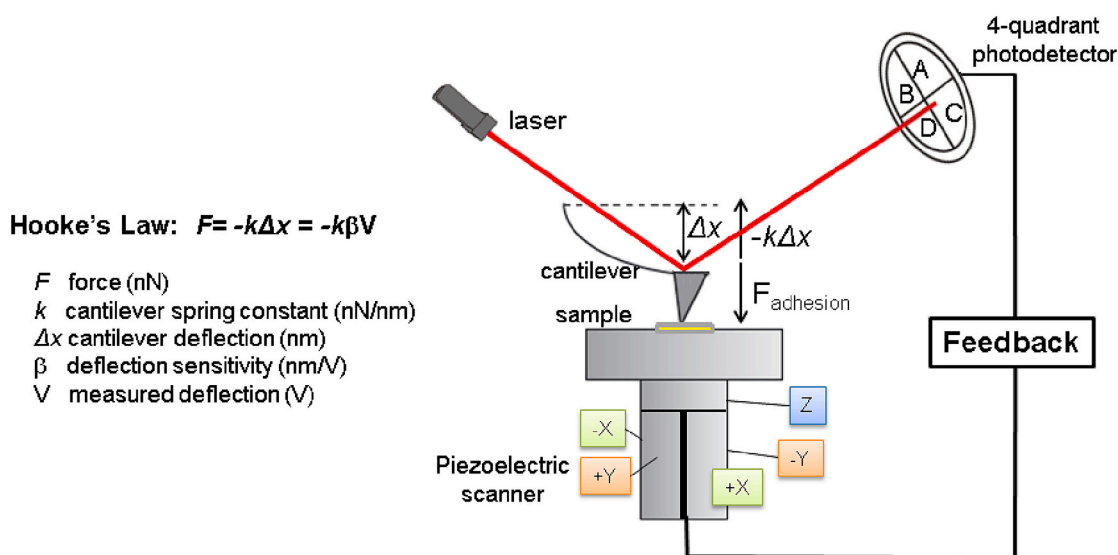


Fig. 1. Schematic diagram of an AFM set-up, where the sample is located on the piezoelectric scanner and based on an optical beam deflection system. In the case of the scanning probe type, it is the tip that is scanning instead of the sample. The scanner is the positioning element allowing 3-D movement with sub-angstrom accuracy: it works by applying voltages to $\pm X$ and $\pm Y$ sectors to move the sample in X and Y directions, respectively; a Z sector moves the sample in the vertical direction. A laser beam strikes on the back-side face of the lever and deflects toward a segmented photodiode. The resulting electrical signal is proportional to the lever deflection and fed into a signal processor, and compared with the desired deflection (set point or feedback parameter). If needed, the voltage applied to the z-piezo is changed to correct the tip-sample distance. Z-piezo can be composed by one or more tubes vertically stacked. The cantilever acts as a small spring, and the deflection can be converted into a force F acting on the cantilever using Hooke's law. As signals are measured in volts, estimation of cantilever deflection sensitivity is required.

measurements because significantly reduce the settling time. Commonly rectangular AFM levers exhibit a higher Q factor compared to triangular cantilevers. To conduct accurate AFM-FS measurements, the proper calibration of the deflection sensitivity and the spring constant of the used cantilever is required. The deflection sensitivity is calibrated to convert the measured volts to nanometers of motion (Fig. 1).

Deflection sensitivity directly relies on the cantilever length and the material of its fabrication. The detector calibration is made by running force-distance (Fz) curves at different local areas of stiff surfaces and calculating the mean slope value of the recorded Fz curves. Freshly cleaved mica surfaces may be also employed for this purpose for AFM cantilevers with soft spring constants. The selected surface to carry out the deflection sensitivity calibration needs to preserve its integrity by preventing indentation by the AFM tip during Fz acquisition. Then, the calibration of the spring constant is done by measuring the motion of the AFM cantilever (assuming it behaves as a harmonic oscillator) in absence of external vibrational excitation. The AFM probe must be retracted from the sample surface when the frequency sweeps. The resonance frequency and Q factor are calculated from the thermal spectrum and the spring constant is obtained by the fitting this response to different models, depending on the specificities of the cantilever. In the case of soft cantilevers (with spring constants usually below of 1 N/m) the most appropriate calculation approach is the thermal tune [115], whereas the Sader's method is commonly employed for cantilevers with larger spring constants (>1 N/m) [116].

Thermal tune is a commonly applied option for those experiments carried out in liquid media where soft cantilevers need to be employed to gain force sensitivity taking advantage to the non-existence of capillarity forces typically exerted in air conditions. It is necessary to point out that there exists an estimation error associated to the determination of the deflection sensitivity based on the fact it is correlated with the spring constant of the lever which in turn is calculated by the free-resonance cantilever thermal spectrum. If the spring constant is accurately calculated by alternative methods like using a vibrometer a correction factor (λ) is estimated to recalibrate the deflection sensitivity. This approach named standardized nanomechanical atomic force

microscopy procedure (SNAP) has been successfully devoted to discern the elastic modulus of polyacrylamide gels minimizing the standard error from 30 % down to 1 % [117]. This methodology is fully suitable for AFM-FS measurements. AFM-FS measurements are ready to be performed once all the above described prerequisites are met. For it, the strong attachment of the two biomolecules that form the complex on a nanoflat surface (typically cleaved mica or gold) and into the AFM tip, respectively, is mandatory –generally covalently- (Fig. 2a). AFM-FS requires the collection of Fz curves where tip-sample interactions are registered in function of piezo displacement for different scanned areas (Fig. 2b). As the formation of complexes is of stochastic nature, only those encounters with a proper orientation of the binding surfaces of the partners will produce successful binding and thus rupture events, so hundreds or thousands Fz require to be taken. Fig. 2b represents a typical force-extension curve for a specific AFM tip-sample interaction. At the start of the cycle, the functionalized tip is far away from the biomolecule-decorated flat surface (Fig. 2b, point 1). The functionalized AFM tip is approached until the van der Waals attractive forces start acting (Fig. 2b, point 2) [118]. This event is also called jump-to-contact [119]. Then, the flexible cantilever bends away from the sample due to repulsive forces until the functionalized tip apex taps the biomolecular-coated surface (Fig. 2b, point 3). These interactions are due to Pauli repulsion and electrostatic repulsive forces. Afterwards, if both molecules specifically recognize each other, they undergo the formation of the complex. In this scenario, the cantilever starts to bend, pulling out both molecules tethered at the AFM tip and on the surface, respectively, until the rupture of the complex (Fig. 2b, point 4).

This unbinding force (F) is directly related to the bonds established and their respective strength. Rupture forces below about 10 pN are hidden by the detection limit of current AFM setups [120]. The length of the stretched crosslinker molecule, used to attach the ligand to the tip, (l_c) coincides with the separation between the extrapolation of the Fz slope and the point when the rupture of the complex takes place. At the end of the cycle, the functionalized tip is at the same position with respect to the beginning of the Fz curve (Fig. 2b, point 5). Successive

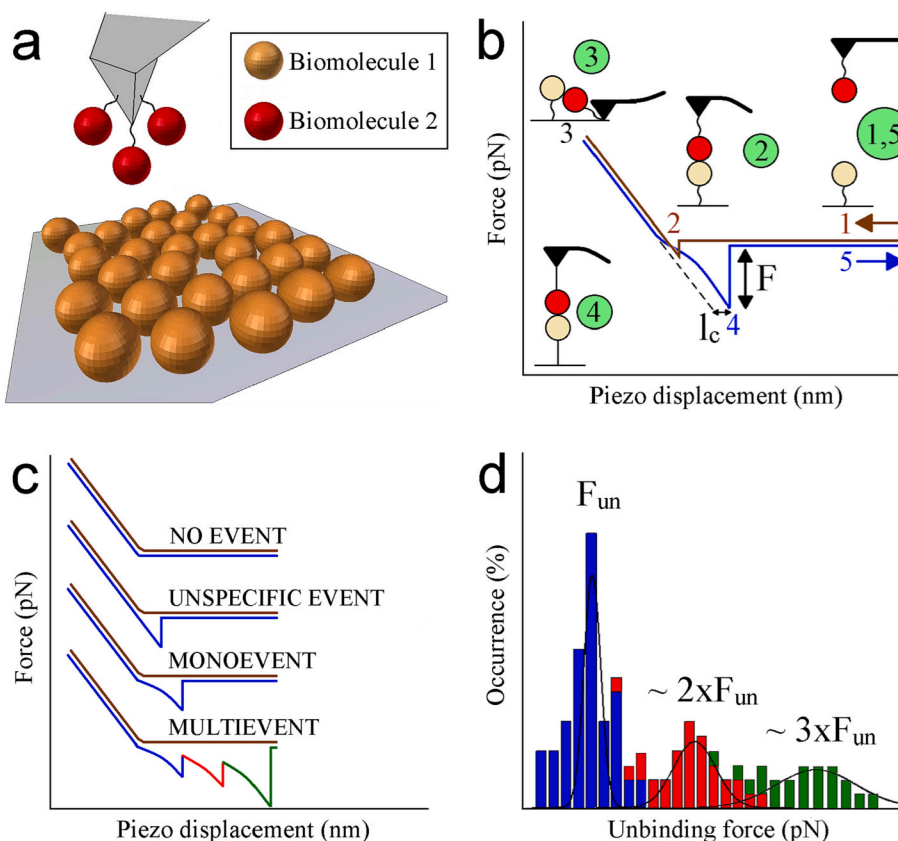


Fig. 2. (a) Schematic representation of AFM-FS for biological studies. (b) Diagram of a typical Fz curve showing a specific biorecognition event between one biomolecule attached to a nanoflat surface and the molecular partner linked onto the AFM tip. Brown arrow indicates the cantilever approach cycle (1–3), whereas the blue arrow depicts the withdrawal from the sample surface (3–5). F and l_c are the unbinding force of the molecular complex and the length of the stretched flexible linker molecule, respectively. Circles representing molecules appear oversized with respect to the lever for a better understanding of the process. (c) Examples of classical Fz curves that can be found in AFM-FS experiments. (d) Conventional statistical analysis of the gathered rupture forces of a complex under a particular experimental condition. Blue, red, and green bars represent the rupture forces when one, two, and three complexes break at the same cycle, respectively. F_{un} is the most probable unbinding force provided by a Gaussian fitting of a distribution of the rupture forces involved in one single complex.

cycles can be taken to different local surface areas following these steps. Fig. 2c illustrates different Fz profiles that can be found during AFM-FS measurements. I) the trace and retrace of the cantilever matches when no events take place. II) Unspecific AFM tip-sample adhesion peaks take place when the retrace displays a linear-shape profile before the rupture point. These Fz curves are discarded for further data analysis. III) the above-described steps are common for single events between both immobilized molecules when the retrace renders a parabolic-shape profile. IV) multiple events can be observed if several biomolecules tethered onto the tip bind to their partners on the surface simultaneously. AFM-FS experiments require to record a large number of Fz curves for each studied condition to conduct reliable statistical analysis since the formation/dissociation of a chemical bond is a stochastic event [121]. Two parameters are required to be checked during force data analysis to unequivocally discern the specific unbinding force events from unspecific tip-sample adhesion forces. First, the length of the fully stretched tether (l_c), which binds the ligand to the tip, should correspond to the theoretical value calculated as the sum of bond distances involved in this linker molecule.

Second, the shape of the Fz observed during the lever retraction before the complex rupture event that, for example, in case the tether used is a polyethylene glycol (PEG) derivative must follow the Worm-like Chain (WLC) model [122]. These two parameters serve as a fingerprint to identify specific rupture events that will be selected to form part in the further force data analysis. Afterward, all the force peaks attributed to specific rupture events from the collected Fz curves are taken into consideration. Then, histograms are plotted to represent the relative occurrence vs. the gained unbinding force values (Fig. 2d).

At this point, it is necessary to introduce that to analyze the forced dissociation of a complex to obtain kinetic parameters, the measuring of force at different loading rates (r_F) is required, and this method is called dynamic force spectroscopy (DFS). Thus, rupture force distributions for different r_F whose fits provide with the most probable rupture forces in a

wide range of r_F will be needed (see Section 4 for more detail). Therefore, this approach enables the identification of the most probable rupture forces for each type of complex formed at specific r_F . Commonly, the leftmost distribution is associated with the rupture force of a single complex (F_{un}). Typically, higher pulling velocity values render broader unbinding force distributions caused by the deformation of the dissociation energy landscapes of the biomolecular complexes analyzed [123]. Blocking experiments are desirable to be conducted to verify if the lower force distribution can be associated to the rupture of a single complex [124]. In a blocking experiment, the AFM-FS measurements are conducted with an excess of free-molecules in solution of the same nature respect to the attached to the AFM tip or at the sample surface. The competition prevents the binding of a part of molecules at the tip or at the surface reducing the number of observed specific events giving the same values but lowering the ratio of successful events and maximizing the ratio of single complex formation respect to multievents. In the last years, it has been evidenced the crucial importance for the proper immobilization of the two partners involved in the process on tip and surface, respectively. For this reason, the following section is based on the discussion of several chemical strategies that have been successfully exploited in previous AFM-FS studies.

3. Functionalization strategies to develop AFM-FS

As for imaging studies it is recommended that the molecules or cells/bacteria particles are separated enough on the sample to be scanned and analyzed individually, AFM-FS require samples that almost completely cover the substrates to increase the probability of meeting and establishing specific interactions with the immobilized ligand at the tip. Additionally, AFM-FS experiments require the strong attachment of the two molecules that form the complex on the tip and surface, respectively. This is based on the weak interactions made when electrostatic forces govern the linkages between biomolecules and solid surfaces.

Biomolecules can be swept when they sense external load forces [125]. To overcome this drawback, covalent functionalization procedures must be developed.

First, the chemical surface modification of the employed materials at the tip and sample is discussed. Nanoflat mica and gold (Au) are today the main suitable substrates to carry out AFM-FS experiments. Muscovite mica is a non-expensive material easy to exfoliate, rendering atomically rough surfaces. Gold substrates have excellent electrical conductivity. For this reason, they are recommended when the AFM-FS measurements are coupled with AFM-SECM or other electrochemical analysis. The most exploited chemical reactivity of gold surfaces is based on the covalent Au-thiol bonds formed when linker molecules ended by sulfhydryl (-SH) moieties are incubated on gold. The most common chemical procedure is the generation of self-assembled monolayers (SAMs) by the reaction between the thiol group from one end of the crosslinker molecule and the gold surface. A vast range of terminal chemical groups could be used at the other end of the linker molecule that will react with the biomolecule of interest. Some examples of appropriate linker molecules dedicated to producing SAMs on gold surfaces to the attachment of carbohydrates (D-Galactosamine) by polyhydroxyethyl acrylamide [126], lipid layers (1-palmitoyl-2-oleoyl-glycerol-3-phosphocholine, POPC and 1,2-dioleoyl-sn-glycerol-3-phosphocholine, DOPC) mediated with citrate molecules [127] and proteins (human thyroid microsome antibodies, Tmab) by N-Hydroxysuccinimide-polyethylene glycol-SH linker molecules [128] on gold nanoparticles. Then, it has been reported chemical modification of gold electrodes by 1,6-hexanedithiol to covalent tether single-stranded DNA and RNA (aptamers) [129]. These functionalization procedures to attach biomolecules could be perfectly extended up to flat gold surfaces. In addition, gold surfaces have the capability to bind directly to those proteins that contain cysteine residues exposed at their outer surface. Nevertheless, it is recommended to design strategies involving linker molecules to increase the distance between the biomolecule of interest and the gold surface and its motion flexibility which enhances the bio-recognition processes with the partner linked into the tip. It is important to avoid hoods or other environments in which silanes or poly(dimethylsiloxane) (PDMS) compounds have been previously used because they can interfere with SAMs formation on gold surfaces [130]. Gold also yields higher quality nanoflat surfaces by flame annealing [131]. In addition to gold, silver (Ag) and copper (Cu) surfaces can be also employed based on the excellent electrical performance being more cost-effective compared to those golden-coated. One of the main drawbacks to use these (Ag/Cu) surfaces is the limited chemical reactivity that can display to covalently attach the biomolecules of interest on them. Alternatively, highly ordered pyrolytic graphite (HOPG) also drives exceptional quality surfaces for conductive studies. HOPG contains uniform structural layers with minimal steps and easily cleaved on smooth surfaces. Recently, HOPG has successfully used to assess the time-lapse DNA mobility in presence of enzymatic proteins [132]. This research could positively contribute on the knowledge of the underlying mechanisms of transcription processes. Other illustrative example is based on the study of amyloidogenic peptide self-aggregation and its orientation [133], which can have strong impact on the early prognosis and clinical treatment of patients with neurodegenerative diseases. Finally, mica surfaces can be also employed for the same purpose. Muscovite mica is a hydrated phyllosilicate mineral of aluminum and potassium ($KAl_2(AlSi_3O_{10})(OH)_2$). Thus, mica chemistry is analogous compared to spontaneous oxidized silicon nitride (Si_3N_4) AFM tips which face silicon oxide (SiO_2) chemical moieties.

The potential AFM tip functionalization strategies are described hereunder. One of the requirements to find suitable crosslinker molecules is their flexibility properties. In this framework, polyethylene glycol (PEG) ($H-[O-CH_2-CH_2]_n-O-H$) arised as a powerful option due to its modular properties [134]. PEG chains do not only undergo stretching under external exerted forces but also are chemically inert, which is highly desirable to prevent unspecific AFM tip-sample interactions

during AFM-FS running experiments [135]. Furthermore, PEG linker molecules exhibit exceptional stability in liquid media, an aspect that aids to lower the tendency of biomolecular aggregation during AFM tip functionalization steps, and remarkably PEG spacers constitute an excellent fingerprint to identify peak forces corresponding to the specific unbinding of the complexes, as explained above. Table 1 recaps the PEG molecules commercially available with their molecular weights (MW) and contour lengths. The reactivity of PEG chains depends on the chemical moieties located at both ends of the crosslinker molecule.

Table 2 depicts the versatile functional groups of different PEG derivatives and their reactivity. It is remarkable to point out that PEG molecules can be synthesized following multitude of alternative geometries (linear, branched, multi-arm, ...) which confer them an enormous richness in terms of crosslinking and conjugation strategies to functionalize AFM tips.

The target groups of carbohydrates, lipids, proteins and DNA/RNA strands are $-COOH/-CHO/-OH$, $-COOH/-OH/-NH_2$, $-COOH/-CHO/-OH/-NH_2/-SH$ and $-CHO/-OH/-NH_2$, respectively. Then, maleimide can serve as intermediate reactive groups to bond biomolecules which expose $-SH$ moieties like cysteine residues via thioether linkages. Finally, the molecular bioconjugation strategies are addressed. In addition to PEG linker chains, a wide variety of short-length hetero-bifunctional linkers are available to exploit the diverse chemistry present in biomolecular surfaces (Fig. 3).

Carboxylic acid (R_1-COOH) based molecular targets can be coupled with 1-Ethyl-3-(3-dimethylaminopropyl)carbodiimide (EDC) linker agent to aminated mica surfaces generated by a mixture of N,N-Diisopropylethylamine (Hünig's base) and (3-Aminopropyl)triethoxylane (APTES) in vapor phase forming a sub-monolayer as reported elsewhere [136] forming covalent amide conjugates ($R_1-CO-NH-R_2$) (Fig. 3a). In addition, EDC can be also employed to label DNA and RNA oligonucleotides through their 5'-phosphate groups creating phosphoramidate linkages (Fig. 3b). EDC has fulfilled the prospects to functionalize AFM tips with factor H proteins [137] or DNA/RNA aptamers [138]. Furthermore, strategies involving EDC as crosslinker molecule for biomolecular conjugation have been also developed for liposomes (lipids) [139], Fibronectin (proteins) [140], DNA [141] or RNA constructs [142].

Aldehyde (R_1-CHO) groups created by periodate oxidation of carbohydrates and proteins can react with hydrazide linker molecules forming hydrazone bonds (Fig. 3c). DNA and RNA strands are susceptible to be also conjugated with hydrazide reagents by reacting their cytosine residues with bisulfite to form reactive sulfone intermediates. The linker reagent more convenient for biological applications is the 3-(2-Pyridyldithio)propionyl hydrazide (PDPH) due to its double reactivity toward the $-CHO$ of the biomolecule of interest and thiolated mica surfaces by terminal hydrazide and pyridyldithio groups, respectively. AFM tip functionalization strategies with hydrazide have rendered promising results with DNA polymerase [143] and maltose binding protein (MBP)/chitin binding protein (CBP) antibodies [144] (proteins) or DNA [145] and RNA strands [146], among others. To our knowledge, there are no studies to date where carbohydrates are covalently

Table 1

PEG models with their respective molecular weight and maximum molecular length when PEG chains are fully extended.

Model	MW (Da)	Contour length (nm)
PEG 200	200	1.3
PEG 400	400	2.5
PEG 1000	1000	6.4
PEG 2000	2000	12.7
PEG 3000	3000	19.1
PEG 4000	4000	25.5
PEG 8000	5000	50.9
PEG 12000	12,000	76.4
PEG 30000	30,000	190.9

Table 2

Chemistry of the terminal functional groups of PEG molecules and their target moieties.

Type	End functional group	Target groups
Aldehyde-PEG	CH ₂ -CH ₂ -CHO	-NH ₂
Amine-PEG	CH ₂ -CH ₂ -NH ₂	-COOH
Aminoxy-PEG	CH ₂ -CH ₂ -ONH ₂	-CHO
Iodoacetamide-PEG	CH ₂ -CH ₂ -NHCO-CH ₂ I	-SH
Maleimide-PEG	CH ₂ -CH ₂ -Maleimide	-SH
N-hydroxysuccinimide (NHS)-PEG	PEG-COO-NHS	-OH, -NH ₂ , -SH ₂
<i>p</i> -Nitrophenyl carbonate-PEG	CH ₂ -CH ₂ -COO- <i>p</i> -Nitrophenyl	-NH ₂
Thiol-PEG	CH ₂ -CH ₂ -SH	-COOH, -Maleimide, -SH

immobilized to AFM tips through hydrazone functionalization protocols.

Nevertheless, several works have reported decorated solid surfaces with carbohydrates [147] or yielding sugar bioconjugation [148], both by exploiting the reactivity of hydrazide linker molecules. Linkers like sulfo-succinimidyl 6-[3'-(2-pyridyldithio)-propionamido] hexanoate (Sulfo-LC-SPDP) rely on excellent bioconjugation results with those proteins which exhibit lysine (R₁-NH₂) or cysteine (R₁-SH₂) superficial residues based on the double reactivity of both ends. The N-hydroxysuccinimide (linker-NHS) terminal group is reactive with primary amines forming amide bonds (R₁-CO-NH-Linker) (Fig. 3d), while the pyridyldithiopropionate (Linker-PDP) after the reduction by agents such as dithiothreitol (DTT) exposes active sulfhydryl groups (Linker-SH) which react with protein cysteine residues forming stable disulfide bonds (Linker-S-S-R₁) (Fig. 3e). NHS moieties from Sulfo-LC-SPDP can also chemically modify mica surfaces after subsequent amination, as above described. Sulfo-LC-SPDP was used to functionalize mica with enzymes and tips with flavoproteins [149]; or covalently attach strept (avidin) protein molecules on mica surfaces [150] or linked into AFM tips [151]. Sometimes, a new procedure has to be design to attach organic molecules, e.g. a coenzyme, as for the covalent attachment of NADP⁺ to AFM tips, where 2-iminothiolane was made to react with the

primary amine of the adenine, creating an amidine derivative carrying a reactive sulfhydryl group in the nanomechanical studies with the enzyme ferredoxin-NADP⁺ reductase [152]. Moreover, it exists many bioconjugation strategies to exploit the -NH₂ target reactivity of liposomes (lipids) [153], salmonella [154] and human epidermal growth factor receptor 2 (HER-2) antibodies (proteins) [155], and DNA/RNA oligos [156].

Another chemical alternative is the use of isocyanate (R₁-N=C=O) moieties with alcohol groups (R₂-OH) to form stable urethane bonds (R₁-NH-COO-R₂) (Fig. 3f). Recently, it has been reported that the use of the heterobifunctional *p*-maleimidophenyl isocyanate (*p*-PMPI) linker molecule to attach cellulose nanocrystals (CNCs) on AFM tip-less levers [157]. This approach has been successfully devoted to addressing the intermolecular interactions of lignocellulosic polymers with CNCs under controlled relative humidity conditions [158] and evaluating the adhesion properties of nanocomposites at different temperatures with these CNCs levers [159]. This technology could aid evolve the next generation of plant-based biofilms with antioxidant [160] or antimicrobial properties [161]. The present functionalization methodology with isocyanate linkers is highly promising to be implemented for biological purposes since many biomolecules are fully covered by external alcohol groups.

The functionalization procedures previously described must be carried out in Teflon (PFTE) beakers protected with a coverslip. This aspect is due to Teflon is a chemically inert material which avoids potential contamination effects during the chemical labeling reactions. To conclude, it is remarkable that although the use of flexible linkers increases the encounter probability, a low percentage of rupture events is generated during AFM-FS experiments, which is caused by a low yield in biorecognition. Typically, the immobilization of biomolecules on tips and solid surfaces is performed randomly. This fact leads to many of the immobilized protein molecules are unable to interact with their partners because their interacting surfaces have been used to anchor them to the substrate, which could negatively interfere in AFM-FS data interpretation rendering small percentages of successful binding events between the biomolecules of interest. Nevertheless, it is possible to introduce the

LINKER MOLECULE	BIOCONJUGATION REACTIVITY	TARGET
a EDC		-COOH
b EDC		-5'-phosphate
c PDPH		-CHO
d Sulfo-LC-SPDP		-NH ₂
e Sulfo-LC-SPDP		-SH
f <i>p</i> -PMPI		-OH

Fig. 3. Schematic representation of chemical functionalization strategies using crosslinker molecules and their reactivity (a) 1-Ethyl-3-(3-dimethylamino-propyl)carbodiimide (EDC) with -COOH target moieties (carbohydrates/lipids/proteins). (b) EDC respect to 5' phosphate groups (DNA/RNA strands). (c) 3-(2-Pyridyldithio)propionyl hydrazide (PDPH) through -CHO groups (carbohydrates/proteins/DNA/RNA). (d) sulfo-succinimidyl 6-[3'-(2-pyridyldithio)-propionamido] hexanoate (Sulfo-LC-SPDP) linker compound conjugation to -NH₂ target groups (lipids/proteins/DNA/RNA). (e) Sulfo-LC-SPDP reactivity to -SH moieties (proteins). *p*-Maleimidophenyl isocyanate (*p*-PMPI) upon -OH target groups (from all types of biomolecules). Red and blue colors indicate the reactivity of the linker molecules toward the solid surface/AFM tip and the biomolecule of interest, respectively. Green circles depict the nature of the formed bonds between the crosslinker molecule and the biomolecule of interest.

factor of protein orientation to measure intermolecular forces and increase thus, the percentage of successful events and then, the quality of AFM-FS. This aim can be achieved for example protecting the binding pocket by forming the transient complex between both biomolecules before the labeling chemical step with the linker molecules. Then, the tagged biomolecules will be isolated by running conventional fast-performance liquid chromatography (FPLC) [136,149]. This implementation can, not only increase notably the percentage of successful events, but also provide some information regarding the specificity in the recognition when different ligands bind to the same binding site of the receptor [149]. The percentage of specific events found in AFM-FS measurements can reach up to 90 % of the total recorded Fz curves when proteins with multivalent binding pockets like the case of the streptavidin protein interacts with its respective biotin ligand [162].

Recently, novel photocleavable linker molecules have been designed and evolved for AFM-FS studies. They are capable to control the release of biomolecules from AFM cantilevers and thus, directly assess molecular binding specificity [163]. In addition, robust molecular fingerprints are required to accurate force spectroscopy data acquisition. Some previous efforts have been devoted in this field like the recent implementation of molecular tethers that incorporate protein domains as the domain 4 from *Dictyostelium discoideum* filamin (ddFLN4) or metalloenzyme polymer chains [164] whose unfolding pattern acts as molecular fingerprint. Albeit this approach is particularly suited to extremely stable molecular complexes that unbind at forces of hundredths or thousands of pN (such as the bacterial adhesins) [165]. Therefore, the study of molecular complexes with lower mechanostabilities (such as the classic biotin:streptavidin interaction) still largely

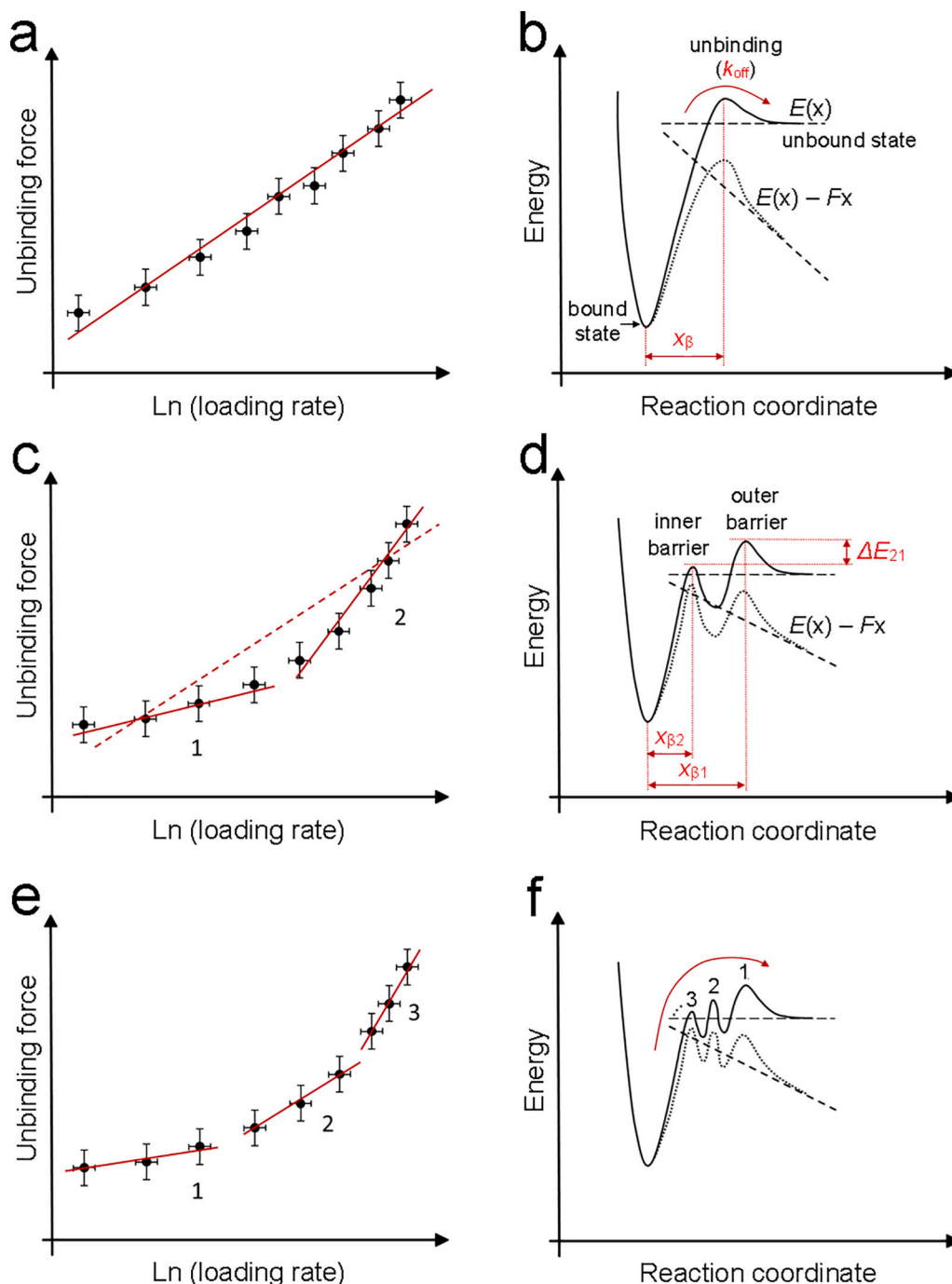


Fig. 4. Schematic illustration of the application of the Bell-Evans model for analysis and interpretation of dynamic force spectroscopy (DFS) results. (a), (c), (e) – representative plots of DFS data and fits with the Bell-Evans model. (b), (d), (f) – conceptual interaction potentials: one-barrier, two-barriers, and multi-barriers, respectively. $E(x)$ – the force-free interaction potential (black solid line), $E(x) - Fx$ – the potential deformed by external force F (black dotted line); x_{β} – the distance between the bound state and the maximum of an activation barrier, ΔE_{21} – the difference between the height of the barriers: outer and inner one.

relies on simple elastic tethers. This approach can be combined with steered molecular dynamic simulation studies in order to elicit the unfolding pathway followed after the stretching [166]. The optimization of suitable protocols for covalent chemical functionalization of flat surfaces and AFM tips with the biomolecule and partner of interest, respectively, enables to conduct AFM-FS measurements properly and gather data with the required quality to discern the adhesion properties of biomolecular systems with the required accuracy.

4. Analysis and interpretation of AFM-FS experimental results

The unbinding force that can be extracted from a force-extension curve (Fig. 2b) expresses the strength of a physical connection (bond) between the AFM tip and the biomolecule of interest in the pulling direction. Although interactions between biomolecules are usually complex, since they result from a combination of several noncovalent interactions, such as electrostatic, van der Waals and hydrophobic interactions, as well as hydrogen bonds, they can be treated as a single (specific) binding in force spectroscopy experiments. A commonly applied model describing a force-induced dissociation of biomolecular complexes is the Bell model [167]. The model assumes that the force applied to the bond lowers the activation barrier and hence facilitates the thermally activated escape from the energy well (Fig. 4b). Thus, the dissociation rate of the biomolecular complex in the presence of loading force (F) is expressed as:

$$k_{\text{off}}(F) = k_{\text{off}}^0 e^{\frac{F x_{\beta}}{k_B T}} \quad (4)$$

where k_{off}^0 is the dissociation rate at zero force, x_{β} is the distance between the bound state and the transition state along the direction of the external pulling force (i.e. the reaction coordinate), k_B is the Boltzmann constant, and T is the absolute temperature.

However, a simple measurement of force curves does not deliver sufficient information on energy landscape of two interacting biomolecules. To deliver thermodynamic and kinetic measures of specific biomolecular interactions, the so-called dynamic force spectroscopy (DFS) is usually applied as above introduced. DFS is based on unbinding force measurements carried out as a function of the loading rate (r_F), a parameter that describes how fast the applied force (F) changes with time (t) during molecular complex unbinding ($r_F \equiv dF/dt$). Evans and Ritchie [168] theoretically explained the observed relationship between the unbinding force and the loading rate. Assuming that r_F is constant, they derived from Eq. (4) the following formula for the most probable unbinding force:

$$F_{\text{un}} = \frac{k_B T}{x_{\beta}} \ln \left(\frac{x_{\beta}}{k_{\text{off}}^0 k_B T r_F} \right) \quad (5)$$

Fitting Eq. (5) to DFS data (Fig. 4a), one can easily extract the values x_{β} and k_{off}^0 . Therefore, the Bell-Evans model has been widely applied to study specific interactions between biomolecules, including the receptor-ligand complexes [169,170]. Table 3 summarizes the unbinding forces and force-free dissociation rates from some relevant biomolecular complexes obtained applying the Bell-Evans model for DFS data [171–197].

The problem arises with more complex DFS data, such as in Fig. 4c. Applying the Bell-Evans model to the entire DFS range (all $F_{\text{un}}(r_F)$ points) results in a low quality fit (low coefficient of determination and high standard deviations of the fitting parameters). Therefore, the DFS range is often divided into two subranges, which are fitted with the model separately [175,176,182,198,199]. This approach results in higher quality fits and is based on the assumption that the molecular complex goes through two activation barriers during unbinding (Fig. 4d): the outer one, which determines the dependency at low loading rates (Fig. 4c, range 1), and the inner one, which determines the dependency at higher loading rates (Fig. 4c, range 2). The inner barrier

Table 3

The unbinding force (F_{un}) of a single complex at a specific loading rate (r_F), the dissociation rate at zero force (k_{off}^0), and the number of fitting regimes for various biomolecular complexes presented in alphabetical order. The values of k_{off}^0 apply to the outer dissociation barrier for those cases with two fitting regimes. N.L. refers to “non-logarithmic” trend.

Biomolecular complex	F_{un} (pN)	r_F (nN/s)	k_{off}^0 (s^{-1})	Number of trends [Ref]
A β :A β	~110	10	12.5	N.L. [171]
Aggrecan:Aggrecan	114 \pm 11	10	0.1	One [172]
$\alpha_v\beta_3$ integrin receptor: RGD peptide	50 \pm 18	1	4.6 $\times 10^{-2}$	One [173]
α -Synuclein ₇₁₋₈₂ : α -Syn ₇₁₋₈₂	~50	10	0.2	One [174]
Antilysozyme:Lysozyme	55 \pm 10	10	1.0 $\times 10^{-3}$	Two [175]
Avidin:Biotin	~55	1	0.35	Two [176]
2Azo-1 DNA strands (Cis)	~30	10	2.2 $\times 10^{-1}$	One [177]
2Azo-1 DNA strands (Trans)	~45	10	3.3 $\times 10^{-2}$	One [177]
Azurin:Cytochrome c551	95 \pm 1	10	14.0	One [178]
4-Heptad coiled coil (CC-A ₄ B ₄): CC-A ₄ B ₄ motifs	~55	10	3.2 $\times 10^{-4}$	One [179]
Colicin:IM9 protein	~70	10	4.9	Two [180]
Concavalin A:Carboxypeptidase A	~145	10	0.2	One [181]
DNA duplex strands	~35	10	1.2	Two [182]
E-cadherin:E-Cadherin	35 \pm 16	10	1.8	One [183]
Epidermal growth factor receptor:GE11	40 \pm 10	1	1.3 $\times 10^{-2}$	One [173]
Ferredoxin NADP ⁺ Reductase (FNR):Ferredoxin	57 \pm 16	10	21.2	One [149]
FNR:Flavodoxin	21 \pm 8	10	55.7	Two [149]
FNR:NADP ⁺	136 \pm 36	10	2.0 $\times 10^{-2}$	One [152]
G-quadruple DNA strands	53 \pm 3	10	1.6	Two [184]
Hemagglutinin:Sialic acid	~60	10	0.7	Two [185]
Human serum albumin (HSA): HSA	~650	10	0.1	One [186]
Lactose:Bovine heart (BHL)	~40	10	9.0 $\times 10^{-2}$	One [187]
Lectin: α -GalNac residues	~245	10	0.8	One [188]
mRNA:HSA	~125	10	0.3	One [189]
Neuraminidase:Sialic acid	~60	10	1.3	One [185]
Oligorotaxanes foldamers	108 \pm 1	10	4.6	N.L. [190]
P53:Azurin	75 \pm 15	10	9.0 $\times 10^{-2}$	One [191]
PDZ domain:Peptide	~120	10	3.0 $\times 10^{-2}$	One [192]
Peptidoglycan:Lysin motif	75 \pm 17	10	0.2	One [193]
RNA strands	~48	10	0.4	One [194]
Streptavidin:Biotin	~170	1	0.6	Two [195]
Transferritin receptor (TfR):T7 peptide	55 \pm 14	1	6.8 $\times 10^{-4}$	One [173]
Vancomycin:D-Ala-D-Ala	~130	10	2.0 $\times 10^{-3}$	One [196]
Von Willebrand Factor A1:A2	~125	10	2.0	One [197]

can be revealed at high loading rates because the outer one is lowered by external force at the moment of force-induced unbinding (Fig. 4d). As a result of the application of the Bell-Evans model to two ranges, x_{β} and k_{off}^0 for each of the barriers as well as the difference between the heights of the barriers (ΔE_{21}) can be obtained (Fig. 4d) [199,200].

It is important to note that the height of the barriers (in relation to the bound state) cannot be determined with this model. The weakness of this approach is the arbitrary way of dividing DFS data into subranges. A larger number of separate subranges, e.g. three instead of two, usually results in a better fitting of the model to experimental data (Fig. 4e). Inference of two, three or more barriers on this basis is highly debatable. In addition, the applicability of the Bell-Evans model is limited for the

following reasons: i) the model reduces all the information about the interaction potential shape to a single parameter – x_β ; ii) it assumes unbinding of a single biomolecular complex; and iii) it ignores rebinding processes. Therefore, more complex theoretical models were developed and applied.

Dudko et al. [201] showed that the phenomenological approach by Evans and Ritchie [168] as well as the microscopic models by Hummer and Szabo [202], and Dudko et al. [203] are particular cases of the more general approach. This unified model, called the Dudko-Hummer-Szabo model, indicates that deviations from the logarithmic nature of the $F_{\text{un}}(r_F)$ dependence seen in Fig. 5a (the same in Fig. 4c and e) may result from the force-dependent energy profile of the transition state. The formula for the unbinding rate constant $k_{\text{off}}(F)$, derived from Kramers' theory [121] under the assumption of a stochastic character of the escape process from the potential well (Eq. (6)) is much more complex than the one proposed by Bell (Eq. (4)):

$$k_{\text{off}}(F) = k_{\text{off}}^0 \frac{\int_{\text{well}} e^{\frac{E(x)-Fx}{k_B T}} dx \int_{\text{barrier}} e^{\frac{-E(x)-Fx}{k_B T}} dx}{\int_{\text{well}} e^{\frac{E(x)}{k_B T}} dx \int_{\text{barrier}} e^{\frac{-E(x)}{k_B T}} dx} \quad (6)$$

The authors specified the free-energy potential shape and obtained the following expression for the most probable unbinding force:

$$F_{\text{un}} = \frac{\Delta G_\beta}{\nu x_\beta} \left\{ 1 - \left[\frac{k_B T}{\Delta G_\beta} \ln \frac{k_{\text{off}}^0 k_B T \exp\left(\frac{\Delta G_\beta}{k_B T}\right)}{x_\beta r_F} \right]^\nu \right\} \quad (7)$$

Here, ΔG_β is the free (Gibbs) energy of activation at zero force and ν is the parameter related to the shape of the free-energy potential. Dudko et al. suggest to use $\nu = 2/3$, appropriate to the linear-cubic free-energy potential, as a universal value in their model [201,204].

The application of this model to the whole range of loading rates results in a high quality fit to the DFS data (Fig. 5a). It is not necessary to distinguish subranges associated with separate activation barriers to justify a course of $F_{\text{un}}(r_F)$ deviating from the logarithmic. The transition through a single barrier (Fig. 5b) can result in the $F_{\text{un}}(r_F)$ dependence as in Fig. 5a. Eq. (7) reduces to Eq. (5) (the Bell-Evans model) for $\nu = 1$ describing an unrealistic case for intermolecular interactions. The Dudko-Hummer-Szabo model, besides its better accuracy, has another advantage over the Bell-Evans model – it enables to extract ΔG_β in addition to k_{off}^0 and x_β . The Dudko-Hummer-Szabo model has been successfully applied to analysis of experimental as well as simulation data for biomolecular interactions [205–207]. However, like the Bell-Evans model, it ignores rebinding processes.

Friddle et al. have considered the contribution of rebinding in the unbinding process [208]. They proposed a model based on Bell's theory, introducing an additional parameter – the equilibrium force (F_{eq}):

$$F_{\text{eq}} = \sqrt{2k_{\text{eff}}\Delta G_{\text{bu}}} \quad (8)$$

Here, k_{eff} is the effective spring constant of the system (the cantilever and the molecular complex) and ΔG_{bu} is the free energy of the unbound state in relation to the bound one. F_{eq} can be interpreted as the force at which the system passes from the near-equilibrium regime to the kinetic one. The most probable unbinding force is approximated by the following formula:

$$F_{\text{un}} \cong F_{\text{eq}} + F_\beta \ln \left(1 + e^{-\gamma} \frac{r_F}{F_\beta k_{\text{off}}(F_{\text{eq}})} \right) \quad (9)$$

where $k_{\text{off}}(F_{\text{eq}})$ is the dissociation rate at the equilibrium force and $\gamma = 0.577$ is the Euler–Mascheroni constant. The parameters: $k_{\text{off}}(F_{\text{eq}})$, x_β , and F_{eq} , which can be recalculated to ΔG_{bu} (Eq. (8)), describe the

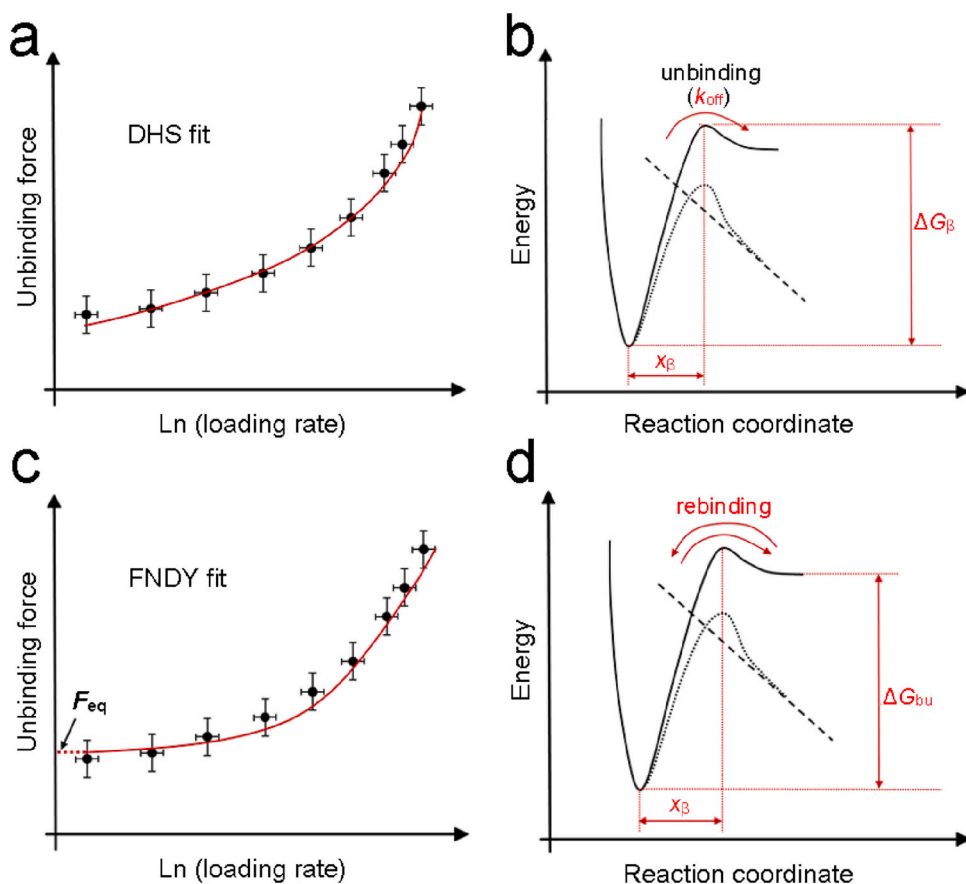


Fig. 5. Schematic illustration of the application of advanced theoretical models for analysis and interpretation of dynamic force spectroscopy (DFS) results. (a), (c) – representative plots of DFS data (the same as in Fig. 4C and D) and fits with the Dudko-Hummer-Szabo (DHS) and the Friddle-Noy-De Yoreo (FNDY) models respectively. (b), (d) – conceptual one-barrier interaction potential: force-free $E(x)$ (black solid line) and deformed by external force $E(x) - Fx$ (black dotted line) with unbinding and rebinding transitions (burgundy arrows). F_{eq} – the equilibrium force (FNDY model), x_β – the distance between the bound state and the maximum of an activation barrier, ΔG_β – the free energy of activation in the absence of external forces, ΔG_{bu} – the free energy of the unbound state relative to the bound state.

kinetics and strength of a bond. The Friddle–Noy–De Yoreo model has been successfully applied to analyze the unfolding process of titin [205], the unbinding of the amyloid- β dimer [209], and the rupture of a single hydrogen bond in the α -helix peptide [210].

In addition to various theoretical models, a methodological framework containing the theoretical models have been proposed to identify possible reasons for the deviations from the logarithmic dependence like: the existence of an inner activation barrier or barriers, the influence of the interaction potential shape, and the contribution of rebinding. The methodology is based on systematic analysis of DFS data for different loading rate ranges with various theoretical models of force induced unbinding [199,203]. Therefore, extending the range of loading rates in particular for high values is a very important issue and several techniques have been proposed [205,211,212].

Beside the methodology based on DFS experiments and the application of theoretical models of force-induced unbinding, another method has been proposed to reconstruct the free energy profile directly from force curves. In AFM-FS experiments, the external force drives the molecular system out of equilibrium, and transitions between bound and unbound states are directly observed as the system settles to a new equilibrium. Such a process can be described by the Jarzynski theorem [213], which is commonly formulated as:

$$e^{-\Delta G_{bu}/k_B T} = \langle e^{-W_i/k_B T} \rangle \quad (10)$$

Here, ΔG_{bu} is the free energy difference between two equilibrium states – bound and unbound, W_i refers to the non-equilibrium work performed for each individual experimental trajectory which interconnects both states, and the angular brackets denote an average over an ensemble of realizations of the process. For example, Harris et al. applied Jarzynski's equality to analyze their single-molecule AFM-FS data and as a result, they reconstructed the free energy surface of mechanical stretching and unfolding of the I27 domain of human cardiac titin [214].

5. Molecular recognition imaging

Biomolecular identification has received considerable attention in recent years due to the increasing interest in identifying or locating individual entities under physiologically relevant conditions. Molecular recognition underlies key biological processes like signaling, immune recognition, and catalysis. Molecular recognition imaging methods rely on scanning with ligand functionalized cantilevers affine to the molecules to be detected on a substrate or directly on cellular/bacterial membranes. Pioneering work was developed in this field by using Topography REcognition imaging (TREC) [215] and tuning-fork-based Transverse Dynamic Force Microscopy (TDFM) [216], albeit both methods lack the ability to provide quantitative information. TREC uses a dynamic mode and feedback loop-based electronics that relates the reduction of the oscillation amplitude with specific interactions between a receptor on the sample and a ligand attached to the AFM tip. Numerous biological systems have been interrogated by TREC, such as avidin: biotin [217], human ether-à-go-go related (hERG) K^+ channels:antibody Kv 11.1 [218], human clusterin:anti-clusterin [219], lipid bilayers [220], among others. TDFM operation consists of oscillating the functionalized AFM tip with tuning forks which are made of quartz materials. TDFM enables the detection of small changes in both the lever oscillation amplitude and the phase contrast between the driving and detected signals. To overcome the aforementioned limitations, force-volume (F–V) [221] emerged as a promising alternative, but the extremely large data acquisition times can lead to drifting effects during image recording. This fact is due to the acquisition and recording of the entire force-curve data for each pixel which composes the image of the scanned surfaces. Recently, disrupted-in-schizophrenia 1 (DISC1) neurological proteins were visualized with anti-DISC1 antibody functionalized tips through molecular recognition maps by F–V [222]. In this framework, the Jumping intermittent force Mode (JM) was presented as a suitable

approach to gather simultaneous topography and adhesion maps at local areas of the scanned biomolecular samples with fast-acquisition times in fluid, as an alternative to dynamic modes [223]. JM takes an Fz curve at each pixel of the image, but collects the height and the maximum tip-sample adhesion force discarding the rest of the Fz data. Using this operational mode by applying very low forces, it is possible to work under the repulsive electrical double layer (REDL) regime. It has been previously demonstrated that REDL induces repulsive interactions between the AFM tip and the external surface of the biomolecule of interest minimizing the non-desirable unspecific tip-sample forces [135,224]. The Debye length (λ_D , nm) is defined by the following equation for 1:1 electrolyte solutions, where the term c defined as the buffer concentration (mol/l) (Eq. (11)) [225,226]:

$$\lambda_D = \left(\frac{0.304}{\sqrt{c}} \right) \quad (11)$$

In these operational terms, the AFM measurements are under the “Derjaguin, Landau, Verwey and Overbeed” (DLVO) conditions (Eq. (12)) [227,228]:

$$\frac{F_0}{\lambda_D} e^{-d/\lambda_D} - \frac{2HR}{3d^3} < k \quad (12)$$

where F_0 is the electrostatic double-layer force amplitude, λ_D the Debye length, H the Hamaker constant, R the radius of the AFM tip apex, d the distance between the tip and the sample surface, and k the spring constant of the cantilever. JM operating in a repulsive regime may solve the three main limitations existing to conduct unequivocal molecular recognition studies, as it avoids unspecific forces allowing to directly obtain the specific unbinding force as the maximum adhesion in the Fz taken at each surface point: I) the lack of quantitative information regarding the studied biomolecular samples; II) long data acquisition times and, III) the potential presence of unspecific tip-sample adhesion forces. JM when applying very low forces has fulfilled high-quality qualitative and quantitative molecular recognition images for avidin by biotinylated probes [135], and FNR scanned using functionalized levers with its redox partners that rendered stronger rupture forces scanned with ferredoxin [136] than for flavodoxin [149].

Recently, JM was probed to discriminate among similar proteins in hybrid strept(avidin) equimolecular samples with a biotinylated AFM tip sensor capable of distinguishing between them in the adhesion maps [150] (Fig. 6). It is expected that the different developed methodologies can be extended up to other biomolecular systems or bacterial/living cell membranes scanned with affine ligand-functionalized AFM tips. The implementation of quantitative molecular recognition good practice protocols may pave the way to go further and contribute to the design and development of high-throughput analytical devices based on force [229], detection signal amplifiers [230], or ultra-sensitive protein tunable biosensors [231], among others.

6. Limitations of AFM and alternatives

Researchers still do not routinely use AFM instrumentation because until recently, such equipment was not easy to employ without expert knowledge, something that it was fixed quite a bit on newer systems. This has been even more difficult when it comes to AFM-FS. Furthermore, the need of functionalization skills, the suitable collection of measurements, a correct data treatment, and finally an understanding of the results, require certain prior knowledge, such as that described here. The present review intends to bring the potentialities of force spectroscopy closer to novice users from biochemistry and biophysics, single-molecule experience researchers and also to potential industrial stakeholders. Moreover, during the different sections that compose this work further details about molecular labeling, AFM tip and substrate functionalization procedures, AFM-FS measurements, analysis with theoretical models of force-induced unbinding, molecular recognition

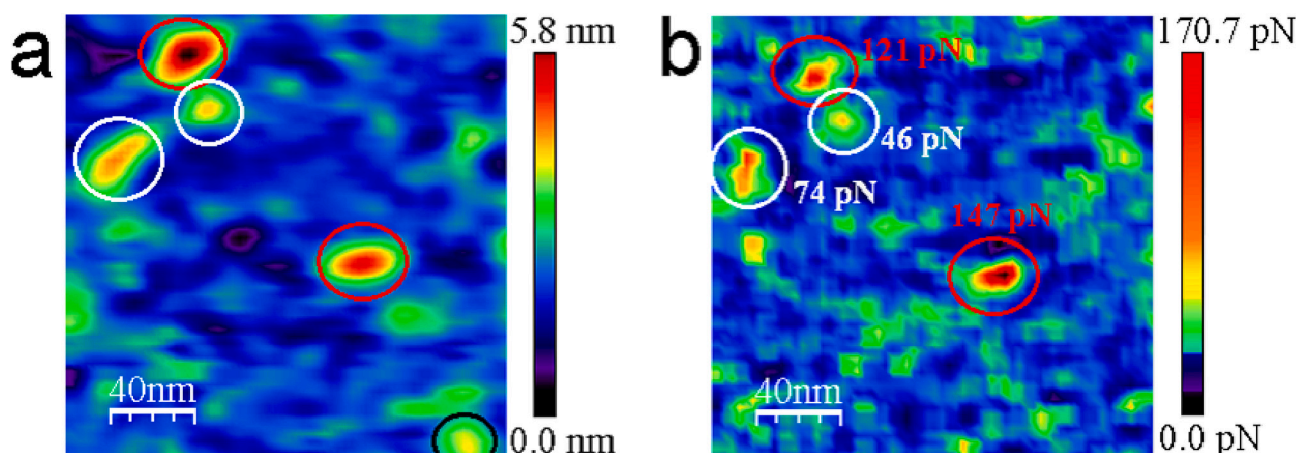


Fig. 6. Topography (a) and adhesion maps (b) of representative molecular recognition AFM images of hybrid strept(avidin) samples with biotinylated tips in buffered conditions. Red, white and black circles represent to streptavidin, avidin and non-identified protein features, respectively. The adhesion events in (b) not only provide the location of the molecules undistinguishable in (a) but also give the unbinding force data at the working loading force. Scan size 200 nm × 200 nm.

imaging and are provided for more advanced users. The described information aims to update, in an understandable way, the procedures and data that involve FS to measure and understand the forces that govern the interactions between molecules in the cellular life. AFM-FS has been presented as suitable technique to gain information on this regard and aid thus, to better understand the underlying mechanical processes that take place during the transient formation/dissociation of biomolecular complexes.

The parameters this technique can provide are mechanical strength, free energy of activation, dissociation rate constant at zero force, distance to the transition state, lifetime of the complex, and number of transitions in the dissociation process. These data allow not only a quantitative comparison with other complexes but also can give an idea of the specificity of the interactions. A single dissociation event is thought to indicate that the complex binds more specifically, and a unique relative orientation is needed to form the complex, while two or more steps indicate a less-specific or more promiscuous binding. These can be seen clearly e.g., in the more specific binding of the enzyme FNR for its physiological partner ferredoxin, than for its replacement in iron-depleting conditions, flavodoxin. Flavodoxin binds to the same interacting surface with a lower strength in a less durable complex, suggesting a dynamic ensemble model [149]. A high mechanical strength and a longer lifetime also relate to a higher molecular affinity. The first nanomechanical study of an enzyme:coenzyme complex reported follows this idea, presenting 136 pN at r_F 10 nNs⁻¹ and a lifetime of 49 s (Table 3) [152]. Generally, the measured unbinding force values reported in the bibliography, for a loading rate of 10 nNs⁻¹, span a wide range, but there are some established relations between data and the character of the complexes. Complexes with dissociation rates higher than 10⁻¹ s⁻¹, and lifetimes shorter than 10 s, are consistent with a relatively high turnover conferring a transient character to these systems [232]. A small distance to the transition state, $x_B \leq 0.1$ nm, likely involves the rupture of hydrogen bonds or salt bridges from a rigid ligand or can be also derived from the simultaneous rupture of several bonds during a single Fz. In this second case, the true value of x_B per single bond is determined by its multiplication by the number of bonds. Whereas, higher $x_B \geq 1$ nm values, presumably implies a deformation of one or both partners before the unbinding [176].

Furthermore, a two-event dissociation process can be assigned to the dissociation of two different parts of the ligand from their corresponding receptor binding sites, as was proposed recently for the 2'-P-AMP and nicotinamide moieties of NADP from their corresponding enzyme bipartite binding sites thanks to using three variants and the wild-type FNR [152]. These data not only show how the binding mechanism occurs but also provide the mechanical parameters at each of these sites.

This could be similar to the proposed existence of two binding sites related to two linear regimes for the interaction between holo-transferrin and its receptor and a single site for the apo-form that corresponds to a single loading rate regime, observing the preference for holo-transferrin, as the average unbinding force was found to be higher than for the complex involving the apo-form [233]. Finally, as we described above, it is possible to obtain the free energy of a complex from the work done by the applied force along several non-equilibrium paths connecting the initial and the final states of a reaction, breaking the gap between non-equilibrium and equilibrium experiments [204].

Currently, the main drawbacks of AFM-FS are I) the inability to accurately measure forces below 10 pN due to its detection limit, II) the inability to discern ultra-fast dissociation processes in nature due to the intrinsic limitations to reach high cantilever velocities and III) the inability to measure at different environmental conditions, e.g. in anaerobiosis. II is especially relevant for those biomolecular transient complexes where their intrinsic reversible binding/unbinding events do not allow the accurate force data acquisition by AFM-FS. Some improvements have been built up in the past years to exceed I and II weaknesses. To overcome the first point, force feedback microscopy (FFM) was designed in the University of Grenoble [234]. FFM employs a force sensor based on a fiber-optic interferometric displacement transducer instead of a laser beam detection system as in commercial AFMs. The advantage of interferometers is the no requirement of mechanical contact with the surface under test. FFM allows to have the full control of the tip-sample interaction avoiding the jump-to-contact between both surfaces. This fact increases the stability and force sensitivity of this technique. Nevertheless, even if FFM has been previously employed to gather information of biological systems in liquid media by pouring a liquid drop on the scanned surface area, it stills requires further development of liquid components like special customized fluid cells and probe holders suitable for liquid operation. It will significantly aid to prevent liquid evaporation during data acquisition and increasing thus, the measurement stability. It is important to remark that AFM has achieved excellent results in air conditions like the measurement of spontaneous water bridges formation between the bare AFM tip apex and freshly cleaved mica surfaces [235]. More research must be devoted in this field to optimize the acquisition of force data in liquid environments which will gain interest to be further exploited for biological purposes. For these reasons, FFM and the previously described optical and magnetic tweezers are complementary methods to AFM. Regarding III, potential technical improvements to control atmosphere, temperature, humidity, and other conditions in sealed chambers will allow to follow interactions under different relevant conditions. For example, operation in anaerobiosis will be relevant for the study of redox

complexes when each partner remains in a specific redox state mimicking nature. Till now this only applied in some cases in a certain state when chemical reductive or oxidants agents kept the specimen of the samples [236] or through the application of an external light with specific excitation wavelengths [237].

Although current AFMs allow studying the conformational changes of biomolecules under certain conditions, for example, weakly immobilized by electrostatic adsorption to provide them with degrees of freedom and movement, if they are molecules that undergo important changes upon ligand binding, these can be observed; thus, enzymatic mechanisms of glycosyltransferases [35,75] or flavoenzymes [73] have been reported supported on these observations. In this sense, the development of high-speed AFM has implemented these capabilities. Smaller z-piezo actuators provide access to high frequencies (up to 130 kHz) to probe the rheological properties of biological samples at high rates [238]. The temporal resolution of HS-AFM can be further increased by designing an ultrafast HS-AFM scanner, as recently showcased in an ultrafast piezoelectric Z-scanner with a record response time two-fold faster than a conventional piezoelectric-based Z-scanner [239]. This type of scanner is capable of scanning different biomolecules such as actin filaments and biological polymers for more than five times faster than conventional Z-scanners. HS-AFM is integrated with an optical beam deflection (OBD) detector for small cantilevers [240]. The AFM image time acquisition is defined by Eq. (13) [241]:

$$t = \left(\frac{2 N^2}{f_c} \right) \quad (13)$$

where t is the acquisition time of the AFM image, f_c is the resonant frequency of the AFM cantilever, and N is the number of pixels per line. Big efforts have been made to design and customize ultrashort cantilevers for HS-AFM measurements [242]. These ultrashort AFM levers enable to break the frontiers of single molecule biophysics and structural biology by enabling the fast performance of Fz curves with μs resolution. All the above-mentioned improvements enable to capture conformational transitions in various biomolecules that occur at infinitesimal time-scales and also the fast collection of Fzs. This aspect is relevant to achieving the required temporal resolution to assess those biological complexes with fast dissociation kinetics. HS-AFM has recently been applied to address the intermolecular adhesion properties of biological systems such as streptavidin:biotin [243,244], or avidin:biotin [245] and intramolecular unfolding events of immunoglobulin titin [205], bacteriorhodopsin proteins [246] or the α -helix unwinding of spectrins [247]. The excellent temporal resolution of HS-AFM enables to visualize those force events related to many still hidden intermediate biomolecular states by classical AFM. Thus, HS-AFM has been employed to determine the molecular dynamics of biomolecular complexes by imaging but has only been demonstrated to serve as proof-of-concept to decipher the nanomechanical properties of biological dissociation processes, while still far from routinely application on this regard, and many efforts are underway to further standardize HS-AFM protocols for force spectroscopy measurements.

7. Conclusions and perspectives

In summary, AFM is one of the most versatile tools currently used in nanoscience. AFM allows performing non-destructive imaging of almost any sample in either air or liquid, regardless of its nature. It can provide topography, mechanical, magnetic, and conductive maps for very different types of samples [248]. This is particularly outstanding in biology as it is the only microscopy technique providing images in aqueous media with nanometric resolution. It also allows for measuring interaction forces between a sharp probe and a sample surface, allowing to probe of the nanomechanical properties of the sample by either applying a controlled force or pulling the sample. Here, we focus on the biological applications of AFM in the FS mode, which go from exerting

high loaded forces to study the nanomechanical properties of a sample through nanoindentation, to the collection of Fzs between ligand functionalized probes and immobilized receptors to form and rupture bonds, or even the simultaneous scanning while taking Fzs to detect molecules at the single level. The fast development of AFM-FS technique and the related functionalization procedures can allow the intermolecular force detection between biomolecules that are part of living cells [249]. The findings obtained by this pioneer approach can open new avenues in the design of more efficient drug carriers or the better knowledge of the underlying mechanisms involved in the cellular uptake mediated pinocytosis. We have shown different modalities of the AFM family that complement AFM-FS data, single-molecule approaches capable of providing data on biomolecule dynamics, and others dedicated to measuring tiny forces without mapping capabilities. AFM-FS provides kinetic parameters, data on the dissociation landscape, and the mechanical forces that maintain biomolecular complexes, which can be determinant in understanding the molecular recognition pathway, binding mechanism and the degree of specificity of the complexes in nature. These data together with those given through imaging as the association pattern or the conformational changes suffered by biomolecules upon ligand binding may be very useful to unravel association/dissociation mechanisms, enzymatic steps, or even the identification of physiological partners or ligands, and its location on natural membranes.

These capabilities together with the promising technical improvements, such as the ones expected from HS-AFM, make AFM-FS a unique tool in nanobiology and other fields. The single-molecule detection capability of AFM-FS together with the possibility to use small amount of samples to perform reliable experiments is promising for the development of FS-based innovative nanobiosensors. Finally, researchers and stakeholders have put a lot of hope in the development of HS-AFM methodologies to obtain very accurate dissociation parameters of transient biological complexes with extremely high unbinding rates in the near future.

CRediT authorship contribution statement

Conceptualization, C.M.; writing-original draft version, A.L., K.L., M. C.P., A.P. and C.M.; writing-review and editing, A.L., K.L., M.C.P., A.P. and C.M. All authors have read and agreed to the published version of the manuscript.

Funding

This research was funded by grant PID2019-103901GB-I00 funded by MCIN/AEI/10.13039/501100011033, grant QTP2103003 funded by CSIC, grants E35_20R and LMP58_18 funded by the Government of Aragón-FEDER, and grant 0512/SBAD/2220 founded by MEiN in Poland.

Declaration of competing interest

The authors declare no conflicts of interest.

Data availability statement

Additional data is available upon reasonable request.

Acknowledgments

A.L. acknowledges ARAID support. A.L., M.C.P. and C.M. would like to acknowledge the use of Servicio General de Apoyo a la Investigación-SAI, Universidad de Zaragoza. A.L., M.C.P. and C.M. acknowledge the use of instrumentation as well as the technical advice provided by the National Facility ELECMI ICTS, node "Laboratorio de Microscopias Avanzadas" at Universidad de Zaragoza. K.L. acknowledges scientific

advice given by Prof. Richard Wong.

References

- [1] M. Delbianco, P. Bharate, S. Varela-Aramburu, P.H. Seeberger, Carbohydrates in supramolecular chemistry, *Chem. Rev.* 116 (4) (2016) 1693–1752, <https://doi.org/10.1021/acs.chemrev.5b00516>.
- [2] E. Fahy, D. Cotter, M. Sud, S. Subramaniam, Lipid classification, structures and tools, *Biochim. Biophys. Acta Mol. Cell Biol Lipids* 1811 (11) (2011) 637–647, <https://doi.org/10.1016/j.bbalip.2011.06.009>.
- [3] B. Kuhlman, P. Bradley, Advances in protein structure prediction and design, *Nat. Rev. Mol. Cell Biol.* 20 (11) (2019) 681–697, <https://doi.org/10.1038/s41580-019-0163-x>.
- [4] X.-W. Wang, C.-X. Liu, L.-L. Chen, Q.C. Zhang, RNA structure probing uncovers RNA structure-dependent biological functions, *Nat. Chem. Biol.* 17 (7) (2021) 755–766, <https://doi.org/10.1038/s41589-021-00805-7>.
- [5] C. Nieuwland, T.A. Hamlin, C. Fonseca Guerra, G. Barone, F.M. Bickelhaupt, B-DNA structure and stability: the role of nucleotide composition and order, *ChemistryOpen* 11 (2) (2022), e202200013, <https://doi.org/10.1002/open.202200013>.
- [6] S. Schefer, M. Oest, S. Rohn, Interactions between phenolic acids, proteins, and carbohydrates-influence on dough and bread properties, *Foods* 10 (11) (2021) 2798, <https://doi.org/10.3390/foods10112798>.
- [7] C. Xu, D.T.W. Ng, Glycosylation-directed quality control of protein folding, *Nat. Rev. Mol. Cell Biol.* 16 (12) (2015) 742–752, <https://doi.org/10.1038/nrm4073>.
- [8] B. Honig, L. Shapiro, Adhesion protein structure, molecular affinities, and principles of cell-cell recognition, *Cell* 181 (3) (2020) 520–535, <https://doi.org/10.1016/j.cell.2020.04.010>.
- [9] J. Li, O. Akil, S.L. Rouse, C.W. McLaughlin, I.R. Matthews, L.R. Lustig, D.K. Chan, E.H. Sherr, Deletion of Tmtc4 activates the unfolded protein response and causes postnatal hearing loss, *J. Clin. Invest.* 128 (11) (2018) 5150–5162, <https://doi.org/10.1172/JCI97498>.
- [10] M. Kanagawa, K. Kobayashi, M. Tajiri, H. Manya, A. Kuga, Y. Yamaguchi, K. Akasaka-Manyu, J.-I. Furukawa, M. Mizuno, H. Kawakami, Y. Shinohara, Y. Wada, T. Endo, T. Toda, Identification of a post-translational modification with ribitol-phosphate and its defect in muscular dystrophy, *Cell Rep.* 14 (9) (2016) 2209–2223, <https://doi.org/10.1016/j.celrep.2016.02.017>.
- [11] J. Jerber, M.S. Zaki, J.Y. Al-Aama, R.O. Rosti, T. Ben-Omran, E. Dikoglu, J. L. Silhavy, C. Caglar, D. Musae, B. Albrecht, et al., Biallelic mutations in TMTC3, encoding a transmembrane and TPR-containing protein, lead to cobblestone lissencephaly, *Am. J. Hum. Genet.* 99 (5) (2016) 1181–1189, <https://doi.org/10.1016/j.ajhg.2016.09.007>.
- [12] Q. Zhai, R. Wang, Q. Lyu, Y. Liu, L.W. Yap, S. Gong, W. Cheng, Mechanically-gated electrochemical ionic channels with chemically modified vertically aligned gold nanowires, *iScience* 24 (11) (2021), 103307, <https://doi.org/10.1016/j.isci.2021.103307>.
- [13] N. Filipczak, J. Pan, S.S.K. Yalamarty, V.P. Torchilin, Recent advancements in liposome technology, *Adv. Drug Deliv. Rev.* 156 (2020) 4–22, <https://doi.org/10.1016/j.addr.2020.06.022>.
- [14] S.T. Eblen, K.D. Tew, P.B. Fisher, Chapter four - extracellular-regulated kinases: signaling from ras to ERK substrates to control biological outcomes, *Adv. Cancer Res.* 138 (2018) 99–142, <https://doi.org/10.1016/bs.acr.2018.02.004>.
- [15] A. Stumpf, T. Brandstetter, J. Hübner, J. Rühle, Hydrogel based protein biochip for parallel detection of biomarkers for diagnosis of a systemic inflammatory response syndrome (SIRS) in human serum, *PLoS One* 14 (12) (2019), e0225525, <https://doi.org/10.1371/journal.pone.0225525>.
- [16] M. Merckx, B. Smith, M. Jewett, Engineering sensor proteins, *ACS Sens.* 4 (12) (2019) 3089–3091, <https://doi.org/10.1021/acssensors.9b02459>.
- [17] T. Nishimura, K. Akiyoshi, Biotransporting biocatalytic reactors toward therapeutic nanofactories, *Adv. Sci.* 5 (11) (2018), 1800801, <https://doi.org/10.1002/advs.201800801>.
- [18] A.L. Tarca, R. Romero, S. Draghici, Analysis of microarray experiments of gene expression profiling, *Am. J. Obstet. Gynecol.* 195 (2) (2006) 373–388, <https://doi.org/10.1016/j.ajog.2006.07.001>.
- [19] D. Gresham, M.J. Dunham, D. Botstein, Comparing whole genomes using DNA microarrays, *Nat. Rev. Genet.* 9 (4) (2008) 291–302, <https://doi.org/10.1038/nrg2335>.
- [20] Y. Wu, J. Yang, Z. Ai, M. Yu, J. Li, S. Li, Identification of key genes and transcription factors in aging mesenchymal stem cells by DNA microarray data, *Gene* 692 (2019) 79–87, <https://doi.org/10.1016/j.gene.2018.12.063>.
- [21] J. Du, H. Qiao, D.-L. Xie, Biomarkers associated with metastasis and prognosis of lung adenocarcinoma based on microarray data, *Gen. Physiol. Biophys.* 41 (3) (2022) 231–243, <https://doi.org/10.4149/gpb.2022009>.
- [22] E. Janzen, C. Blanco, H. Peng, J. Kenchel, I.A. Chen, Promiscuous ribozymes and their proposed role in prebiotic evolution, *Chem. Rev.* 120 (11) (2020) 4879–4897, <https://doi.org/10.1021/acs.chemrev.9b00620>.
- [23] P.B. Dykstra, M. Kaplan, C.D. Smolke, Engineering synthetic RNA devices for cell control, *Nat. Rev. Genet.* 23 (4) (2020) 215–228, <https://doi.org/10.1038/s41576-021-00436-7>.
- [24] S. Müller, D. Strohbach, J. Wolf, Sensors made of RNA: tailored ribozymes for detection of small organic molecules, metals, nucleic acids and proteins, *IEE Proc. Nanobiotechnol.* 153 (2) (2006) 31–40, <https://doi.org/10.1049/ip-nbt:20050047>.
- [25] M. You, J.L. Litke, R. Wu, S.R. Jaffrey, Detection of low-abundance metabolites in live cells using an RNA integrator, *Cell Chem. Biol.* 26 (4) (2019) 471–481, <https://doi.org/10.1016/j.chembiol.2019.01.005>.
- [26] H.H. Nguyen, J. Park, S. Kang, M. Kim, Surface plasmon resonance: a versatile technique for biosensor applications, *Sensors* 15 (5) (2015) 10481–10510, <https://doi.org/10.3390/s150510481>.
- [27] I. Jakobowska, F. Becker, S. Minguzzi, K. Hansen, B. Henke, N.H. Epalle, E. Beitz, S. Hannus, Fluorescence cross-correlation spectroscopy yields true affinity and binding kinetics of plasmodium lactate transport inhibitors, *Pharmaceuticals* 14 (8) (2021) 757, <https://doi.org/10.3390/ph14080757>.
- [28] T. Kawanobe, N. Shiranaga, N. Kioka, Y. Kimura, K. Ueda, Apolipoprotein A-I directly interacts with extracellular domain 1 of human ABCA1, *Biosci. Biotechnol. Biochem.* 83 (3) (2019) 490–497, <https://doi.org/10.1080/09168451.2018.1547106>.
- [29] E.W.E. Verweij, R. Bosma, M. Gao, J. van den Bor, B. Al Araaj, S.M. de Munnik, X. Ma, R. Leurs, H.F. Vischer, BRET-based biosensors to measure agonist efficacies in histamine H1 receptor-mediated G protein activation, signaling and interactions with GRKs and β -arrestins, *Int. J. Mol. Sci.* 23 (6) (2022) 3184, <https://doi.org/10.3390/ijms23063184>.
- [30] O.J. Wilkinson, C. Carrasco, C. Aicart-Ramos, F. Moreno-Herrero, M. S. Dillingham, Bulk and single-molecule analysis of a bacterial DNA2-like helicase-nuclease reveals a single-stranded DNA looping motor, *Nucleic Acids Res.* 48 (14) (2020) 7991–8005, <https://doi.org/10.1093/nar/gkaa562>.
- [31] H. Wang, F. Zhou, Y. Guo, L.A. Ju, Micropipette-based biomechanical nanotools on living cells, *Eur. Biophys. J.* 51 (2) (2022) 119–133, <https://doi.org/10.1007/s00249-021-01587-5>.
- [32] L. Limozin, K. Sengupta, Quantitative reflection interference contrast microscopy (RICM) in soft matter and cell adhesion, *ChemPhysChem* 10 (16) (2009) 2752–2768, <https://doi.org/10.1002/cphc.200900601>.
- [33] L. Ju, Y. Chen, K. Li, Z. Yuan, B. Liu, S.P. Jackson, C. Zhu, Dual biomembrane force probe enables single-cell mechanical analysis of signal crosstalk between multiple molecular species, *Sci. Rep.* 7 (1) (2017) 14185, <https://doi.org/10.1038/s41598-017-13793-3>.
- [34] D.K. Sasmal, L.E. Pulido, S. Kasal, J. Huang, Single-molecule fluorescence resonance energy transfer in molecular biology, *Nanoscale* 8 (2016) 19928–19944, <https://doi.org/10.1039/c6nr06794h>.
- [35] E. Lira-Navarrete, M.C. Pallarés, F. Castello, M.J. Ruedas-Rama, A. Orte, A. Lostao, R. Hurtado-Guerrero, Protein O-fucosyltransferase 1 undergoes interdomain flexibility in solution, *Molecules* 26 (8) (2021) 2105, <https://doi.org/10.3390/molecules26082105>.
- [36] C.J. Bustamante, Y.R. Chemla, S. Liu, M.D. Wang, Optical tweezers in single-molecule biophysics, *Nat. Rev. Methods Primers* 1 (2021) 25, <https://doi.org/10.1038/s43586-021-00021-6>.
- [37] H. Yin, M.D. Wang, K. Svoboda, R. Landick, S.M. Block, J. Gelles, Transcription against an applied force, *Science* 270 (5242) (1995) 1653–1657, <https://doi.org/10.1126/science.270.5242.1653>.
- [38] M.G.M. Van Rosmalen, D. Kamsma, A.S. Biebricher, C. Li, A. Zlotnick, W.H. Roos, G.J.L. Wuite, Revealing in real-time a multistep assembly mechanism for SV40 virus-like particles, *Sci. Adv.* 6 (16) (2020), eaaz1639, <https://doi.org/10.1126/sciadv.aaz1639>.
- [39] K. Lehmann, M. Shayegan, G.A. Blab, N.R. Forde, Optical tweezers approaches for probing multiscale protein mechanics and assembly, *Front. Mol. Biosci.* 7 (2020), 577314, <https://doi.org/10.3389/fmolb.2020.577314>.
- [40] T.A. Springer, von Willebrand factor, Jedi knight of the bloodstream, *Blood* 124 (9) (2014) 1412–1425, <https://doi.org/10.1182/blood-2014-05-378638>.
- [41] P. Kate-Andrew, A. Raudsepp, D. Fan, U. Stauffer, M.A.K. Williams, E. Avci, Optical microlever assisted DNA stretching, *Opt. Express* 29 (16) (2021) 25836–25847, <https://doi.org/10.1364/OE.430465>.
- [42] D.B. Ritchie, M.T. Woodside, Probing the structural dynamics of proteins and nucleic acids with optical tweezers, *Curr. Opin. Struct. Biol.* 34 (2015) 43–51, <https://doi.org/10.1016/j.sbi.2015.06.006>.
- [43] J. Kim, N.E. Hudson, T.A. Springer, Force-induced on-rate switching and modulation by mutations in gain-of-function von Willebrand diseases, *Proc. Natl. Acad. Sci. U. S. A.* 112 (15) (2015) 4648–4653, <https://doi.org/10.1073/pnas.1501689112>.
- [44] P. Pokhrel, S. Sasaki, C. Hu, D. Karna, S. Pandey, Y. Ma, K. Nagasawa, H. Mao, Single-molecule displacement assay reveals strong binding of polyvalent dendrimer ligands to telomeric G-quadruplex, *Anal. Biochem.* 649 (2022), 114693, <https://doi.org/10.1016/j.ab.2022.114693>.
- [45] K.R. Peddireddy, D. Michieletto, G. Aguirre, J. Garamella, P. Khanal, R. M. Robertson-Anderson, DNA conformation dictates strength and flocculation in DNA-microtubule composites, *ACS Macro Lett.* 10 (12) (2021) 1540–1548, <https://doi.org/10.1021/acsmacrolett.1c00638>.
- [46] S. Kono, A. van den Berg, M. Simonetta, A. Mukhortava, E.F. Garman, I. Tesser, Resolving the subtle details of human DNA alkyltransferase lesion search and repair mechanism by single-molecule studies, *Proc. Natl. Acad. U.S.A.* 119 (11) (2022), e2116218119, <https://doi.org/10.1073/pnas.2116218119>.
- [47] Y.-L. Chen, J.-D. Wen, Translation initiation site of mRNA is selected through dynamic interaction with the ribosome, *Proc. Natl. Sci. U. S. A.* 119 (22) (2022), e2118099119, <https://doi.org/10.1073/pnas.2118099119>.
- [48] J. Ma, L. Bai, M.D. Wang, Transcription under torsion, *Science* 340 (6140) (2013) 1580–1583, <https://doi.org/10.1126/science.1235441>.
- [49] M.D. Newton, B.J. Taylor, R.P.C. Drissen, L. Roos, N. Cveticic, S. Allynjaun, B. Lenhard, M.E. Cuomo, D.S. Rueda, DNA stretching induces Cas9 off-target activity, *Nat. Struct. Mol. Biol.* 26 (3) (2019) 185–192, <https://doi.org/10.1038/s41594-019-0188-z>.

- [50] T.R. Strick, J.F. Allemand, D. Bensimon, V. Croquette, Behavior of supercoiled DNA, *Biophys. J.* 74 (4) (1998) 2016–2028, [https://doi.org/10.1016/S0006-3495\(98\)77908-1](https://doi.org/10.1016/S0006-3495(98)77908-1).
- [51] C. Gosse, V. Croquette, Magnetic tweezers: micromanipulation and force measurement at the molecular level, *Biophys. J.* 82 (6) (2002) 3314–3329, [https://doi.org/10.1016/S0006-3495\(02\)75672-5](https://doi.org/10.1016/S0006-3495(02)75672-5).
- [52] E.C. Eckels, S. Haldar, R. Tapia-Rojo, J.A. Rivas-Pardo, J.M. Fernández, The mechanical power of titin folding, *Cell Rep.* 27 (6) (2019) 1836–1847, <https://doi.org/10.1016/j.celrep.2019.04.046>.
- [53] R. Tapia-Rojo, E.C. Eckels, J.M. Fernández, Ephemeral states in protein folding under force captured with a magnetic tweezers design, *Proc. Natl. Acad. Sci. U. S. A.* 116 (16) (2019) 7873–7878, <https://doi.org/10.1073/pnas.1821284116>.
- [54] N. Li, J. Wang, K. Ma, L. Liang, L. Mi, W. Huang, X. Ma, Z. Wang, W. Zheng, L. Xu, et al., The dynamics of forming a triplez in an artificial telomere inferred by DNA mechanics, *Nucleic Acids Res.* 47 (15) (2019) e86, <https://doi.org/10.1093/nar/gkz464>.
- [55] R. Tapia-Rojo, A. Alonso-Caballero, J.M. Fernandez, Direct observation of a coil-to-helix contraction triggered by vinculin binding to talin, *Sci. Adv.* 6 (21) (2020), eaaz4707, <https://doi.org/10.1126/sciadv.aaz4707>.
- [56] S. Hormeno, O.J. Wilkinson, C. Aicart-Ramos, S. Kuppa, E. Antony, M. S. Dillingham, F. Moreno-Herrero, Human HELB is a processive motor protein that catalyzes RPA clearance from single-stranded DNA, *Proc. Natl. Acad. Sci. U. S. A.* 119 (15) (2022), e2112376119, <https://doi.org/10.1073/pnas.2112376119>.
- [57] G. Binnig, C.F. Quate, C. Gerber, Atomic force microscope, *Phys. Rev. Lett.* 56 (1986) 930–933, <https://doi.org/10.1103/PhysRevLett.56.930>.
- [58] S.J. Eppell, M. Feinstein, L. Li, B. White, F.R. Zypman, Signal distortion in atomic force microscopy photodetector, *Rev. Sci. Instrum.* 88 (10) (2017), 103703, <https://doi.org/10.1063/1.5008833>.
- [59] M. Dukic, V. Todorov, S. Andany, A.P. Nievergelt, C. Yang, N. Hosseini, G. E. Fantner, Digitally controlled analog proportional-integral-derivative (PID) controller for high-speed scanning probe microscopy, *Rev. Sci. Instrum.* 88 (12) (2017), 123712, <https://doi.org/10.1063/1.5010181>.
- [60] P.K. Hansma, J.P. Cleveland, M. Radmacher, D.A. Walters, P.E. Hillner, M. Bezanilla, M. Fritz, D. Vie, H.G. Hansma, Tapping mode atomic force microscopy in liquids, *Appl. Phys. Lett.* 64 (1994) 1738, <https://doi.org/10.1063/1.111795>.
- [61] T. Sulchek, R. Hsieh, J.D. Adams, S.C. Minne, C.F. Quate, High-speed atomic force microscopy in liquid, *Rev. Sci. Instrum.* 71 (2000) 2097, <https://doi.org/10.1063/1.1150586>.
- [62] B.T. Bajar, E.S. Wang, S. Zhang, M.Z. Lin, J.A. Chu, Guide to fluorescent protein FRET pairs, *Sensors* 16 (9) (2016) 1488, <https://doi.org/10.3390/s16091488>.
- [63] Y. Zhang, T. Huang, D.M. Jorgens, A. Nickerson, L.-J. Lin, J. Pelz, J.W. Gray, C. S. López, X. Nan, Quantitating morphological changes in biological samples during scanning electron microscopy sample preparation with correlative super-resolution microscopy, *PLoS One* 12 (5) (2017), e0176839, <https://doi.org/10.1371/journal.pone.0176839>.
- [64] A.J. Hobro, N.I. Smith, An evaluation of fixation methods: spatial and compositional cellular changes observed by Raman imaging, *Vib. Spectrosc.* 91 (2017) 31–45, <https://doi.org/10.1016/j.vibspec.2016.10.012>.
- [65] Y.F. Dufrene, T. Ando, R. Garcia, D. Alsteens, D. Martinez-Martin, A. Engel, C. Gerber, D.J. Müller, Imaging modes of atomic force microscopy for application in molecular and cell biology, *Nat. Nanotechnol.* 12 (4) (2017) 295–307, <https://doi.org/10.1038/nnano.2017.45>.
- [66] M. Li, X. Xi, L. Liu, Peak force tapping atomic force microscopy for advancing cell and molecular biology, *Nanoscale* 13 (2021) 8358–8375, <https://doi.org/10.1039/d1nr01303c>.
- [67] K. Meinander, T.N. Jensen, S.B. Simonsen, S. Helveg, J.V. Lauritsen, Quantification of tip-broadening in non-contact atomic force microscopy with carbon nanotube tips, *Nanotechnology* 23 (40) (2012), 405705, <https://doi.org/10.1088/0957-4484/23/40/405705>.
- [68] N.I. Abu-Lail, T.A. Camesano, Polysaccharide properties probed with atomic force microscopy, *J. Microsc.* 212 (Pt3) (2003) 217–238, <https://doi.org/10.1111/j.1365-2818.2003.01261.x>.
- [69] T. Fukuma, M.J. Higgins, S.P. Jarvis, Direct imaging of individual intrinsic hydration layers on lipid bilayers at Angstrom resolution, *Biophys. J.* 92 (10) (2007) 3603–3609, <https://doi.org/10.1529/biophysj.106.100651>.
- [70] R. Villanueva, P. Ferreira, C. Marcuello, A. Usón, M.D. Miramar, M.L. Peleato, A. Lostao, S.A. Susin, M. Medina, Key residues regulating the reductase activity of the human mitochondrial apoptosis inducing factor, *Biochemistry* 54 (33) (2015) 5175–5184, <https://doi.org/10.1021/acs.biochem.5b00696>.
- [71] M. Sebastián, E. Lira-Navarrete, A. Serrano, C. Marcuello, A. Velázquez-Campoy, A. Lostao, R. Hurtado-Guerrero, M. Medina, M. Martínez-Júlviz, The FAD synthetase from the human pathogen *Streptococcus pneumoniae*: a bifunctional enzyme exhibiting activity-dependent redox requirements, *Sci. Rep.* 7 (1) (2017) 7609, <https://doi.org/10.1038/s41598-017-07716-5>.
- [72] C. Marcuello, G.A. Frempong, M. Balsaera, M. Medina, A. Lostao, Atomic force microscopy to elicit conformational transitions of ferredoxin-dependent flavin thioredoxin reductases, *Antioxidants* 10 (9) (2021) 1437, <https://doi.org/10.3390/antiox10091437>.
- [73] N. Novo, R. Romero-Tamayo, C. Marcuello, S. Boneta, I. Blasco-Machin, A. Velázquez-Campoy, R. Villanueva, R. Moreno-Loshuertos, A. Lostao, M. Medina, et al., Beyond a platform protein for the degradosome assembly: the apoptosis inducing factor as efficient nuclease involved in chromatinolysis, *PNAS Nexus* (2023), pgac312, <https://doi.org/10.1093/pnasnexus/pgac312>.
- [74] L. Ceballos-Laita, C. Marcuello, A. Lostao, L. Calvo-Begueria, A. Velázquez-Campoy, M.T. Bes, M.F. Fillat, M.-L. Peleato, Microcystin-LR binds iron, and iron promotes self-assembly, *Environ. Sci. Technol.* 51 (9) (2017) 4841, <https://doi.org/10.1021/acs.est.6b05939>.
- [75] E. Lira-Navarrete, M. de Las Rivas, I. Compañón, M.C. Pallarés, Y. Kong, J. Iglesias-Fernández, G.J.L. Bernardes, J.M. Peregrina, C. Rovira, P. Bernadó, et al., Dynamic interplay between catalytic and lectin domains of GalNAc-transferases modulates protein O-glycosylation, *Nat. Commun.* 6 (2015) 6937, <https://doi.org/10.1038/ncomms7937>.
- [76] E. Lipiec, K. Sofinska, S. Seweryn, M. Wilkosz, M. Szymonski, Revealing DNA structure at liquid/solid interfaces by AFM-based high-resolution imaging and molecular spectroscopy, *Molecules* 26 (21) (2021) 6476, <https://doi.org/10.3390/molecules26216476>.
- [77] P. Ares, M.E. Fuentes-Pérez, E. Herrero-Galán, J.M. Valpuesta, A. Gil, J. M. Gómez-Herrero, F. Moreno-Herrero, High resolution atomic force microscopy of double-stranded RNA, *Nanoscale* 8 (2016) 11818–11826, <https://doi.org/10.1039/C5NR07445B>.
- [78] A. Alessandrini, P. Facci, Unraveling lipid/protein interaction in model lipid bilayers by atomic force microscopy, *J. Mol. Recognit.* 24 (3) (2011) 387–396, <https://doi.org/10.1002/jmr.1083>.
- [79] M.C. Pallarés, C. Marcuello, L. Botello-Morte, A. González, M.F. Fillat, A. Lostao, Sequential binding of FurA from *Anabaena* sp. PCC 7120 to iron boxes: exploring regulation at the nanoscale, *Biochim. Biophys. Acta* 1844 (3) (2014) 623–631, <https://doi.org/10.1016/j.bbapap.2014.01.005>.
- [80] V.C. Sein-Echaluce, M.C. Pallarés, A. Lostao, I. Yruela, A. Velázquez-Campoy, M. L. Peleato, M. Fillat, Molecular basis for the integration of environmental signals by FurB from *Anabaena* sp. PCC 7120, *Biochem. J.* 475 (1) (2018) 151–168, <https://doi.org/10.1042/BCJ20170692>.
- [81] M.B. Viani, T.E. Schäffer, G.T. Palocz, L.L. Pietrasanta, B.L. Smith, J. B. Thompson, M. Richter, M. Rief, H.E. Gaub, K.W. Plaxco, et al., Fast imaging and fast force spectroscopy of single biopolymers with a new atomic force microscope designed for small cantilevers, *Rev. Sci. Instrum.* 70 (11) (1999) 4300–4303, <https://doi.org/10.1063/1.1150069>.
- [82] K. Lim, G. Nishide, T. Yoshida, T. Watanabe-Nakayama, A. Kobayashi, M. Hazawa, R. Hanayama, T. Ando, R.W. Wong, Millisecond dynamic of SARS-CoV-2 spike and its interaction with ACE2 receptor and small extracellular vesicles, *J. Extracell. Vesicles* 10 (14) (2021), e12170, <https://doi.org/10.1002/jev2.12170>.
- [83] K.S. Lim, M.S. Mohamed, H. Wang, M. Hartono, A. Hazawa, D.C.-C. Voon Kobayashi, N. Kodera, T. Ando, R.W. Wong, Direct visualization of avian influenza H5N1 hemagglutinin precursor and its conformational change by high-speed atomic force microscopy, *Biochim. Biophys. Acta Gen. Subj.* 1864 (2) (2020), 129313, <https://doi.org/10.1016/j.bbagen.2019.02.015>.
- [84] K. Lim, N. Kodera, H. Wang, M.S. Mohamed, M. Hazawa, A. Kobayashi, T. Yoshida, R. Hanayama, S. Yano, T. Ando, R.W. Wong, High-speed AFM reveals molecular dynamics of human influenza A hemagglutinin and its interaction with exosomes, *Nano Lett.* 20 (9) (2020) 6320–6328, <https://doi.org/10.1021/acs.nanolett.0c01755>.
- [85] A. Valbuena, S. Maity, M.G. Mateu, W.H. Roos, Visualization of single molecules building a viral capsid protein lattice through stochastic pathways, *ACS Nano* 14 (7) (2020) 8724–8734, <https://doi.org/10.1021/acsnano.0c03207>.
- [86] N. Kodera, D. Noshiro, S.K. Dora, T. Mori, J. Habchi, D. Blocquel, A. Gruet, M. Dosson, E. Salladini, C. Bignon, et al., Structural and dynamics analysis of intrinsically disordered proteins by high-speed atomic force microscopy, *Nat. Nanotechnol.* 16 (2) (2021) 181–189, <https://doi.org/10.1038/s41565-020-00798-9>.
- [87] G. Nishide, K. Lim, M.S. Mohamed, A. Kobayashi, M. Hazawa, T. Watanabe-Nakayama, N. Kodera, T. Ando, R.W. Wong, High-speed atomic force microscopy reveals spatiotemporal dynamics of histone protein H2A involution by DNA inchworming, *J. Phys. Chem. Lett.* 12 (15) (2021) 3837–3846, <https://doi.org/10.1021/acs.jpcclett.1c00697>.
- [88] J. Junyer, R. Evans, A. Pritzel, T. Green, M. Figurnov, O. Ronneberger, K. Tunyasuvunakool, R. Bates, A. Židek, A. Potapenko, et al., Highly accurate protein structure prediction with AlphaFold, *Nature* 596 (7873) (2021) 583–589, <https://doi.org/10.1038/s41586-021-03819-2>.
- [89] M. Baek, F. DiMaio, I. Anishchenko, J. Dauparas, S. Ovchinnikov, G.R. Lee, J. Wang, Q. Cong, L.N. Kinch, R.D. Schaeffer, Accurate prediction of protein structures and interactions using a three-track neural network, *Science* 373 (6557) (2021) 871–876, <https://doi.org/10.1126/science.abbj8754>.
- [90] M.S. Mohamed, A. Kobayashi, A. Taoka, T. Watanabe-Nakayama, Y. Kikuchi, M. Hazawa, T. Minamoto, Y. Fukumori, N. Kodera, T. Uchihashi, et al., High-speed atomic force microscopy reveals loss of nuclear pore resilience as a dying code in colorectal cancer cells, *ACS Nano* 11 (6) (2017) 5567–5578, <https://doi.org/10.1021/acsnano.7b00906>.
- [91] M.S. Mohamed, M. Hazawa, A. Kobayashi, L. Guillaud, T. Watanabe-Nakayama, M. Nakayama, H. Wang, N. Kodera, M. Oshima, T. Ando, et al., Spatiotemporally tracking of nano-biofilaments inside the nuclear pore complex core, *Biomaterials* 256 (2020), 120198, <https://doi.org/10.1016/j.biomaterials.2020.120198>.
- [92] H. Yamashita, A. Taoka, T. Uchihashi, T. Asano, T. Ando, Y. Fukumori, Single-molecule imaging on living bacterial cell surface by high-speed AFM, *J. Mol. Biol.* 422 (2) (2012) 300–309, <https://doi.org/10.1016/j.jmb.2012.05.018>.
- [93] K. Kobayashi, N. Kodera, T. Kasai, Y.O. Tahara, T. Toyonaga, M. Mizutani, I. Fujiwara, T. Ando, M. Miyata, Movements of mycoplasma mobile gliding machinery detected by high-speed atomic force microscopy, *mBio* 12 (3) (2021), e0004021, <https://doi.org/10.1128/mBio.00040-21>.

- [94] M. Shibata, T. Uchihashi, T. Ando, R. Yasuda, Long-tip high-speed atomic force microscopy for nanometer-scale imaging in live cells, *Sci. Rep.* 5 (2015) 8724, <https://doi.org/10.1038/srep08724>.
- [95] C. Feuille, E. Lambert, M. Ewald, M. Azouz, S. Henry, S. Marsaudon, C. Cullin, S. Lecomte, M. Molinari, High speed AFM and nanoinfrared spectroscopy investigation of A β 1-42 peptide variants and their interaction with POPC/SM/Chol/GM1 model membranes, *Front. Mol. Biosci.* 7 (2020), 571696, <https://doi.org/10.3389/fmolb.2020.571696>.
- [96] A. Dazzi, R. Prazeres, F. Glotin, J.M. Ortega, Analysis of nano-chemical mapping of performed by an AFM-based ("AFMIR") acousto-optic technique, *Ultramicroscopy* 107 (12) (2007) 1194–1200, <https://doi.org/10.1016/j.ultramicro.2007.01.018>.
- [97] S. Clède, F. Lambert, C. Sandt, S. Kascakova, M. Unger, E. Harté, M.-A. Plamont, R. Saint-Fort, A.D. Besseau, Z. Gueroui, et al., Detection of an estrogen derivative in two breast cancer cell lines using a single core multimodal probe for imaging (SComPI) imaged by a panel of luminescent and vibrational techniques, *Analyst* 138 (19) (2013) 5627–5638, <https://doi.org/10.1039/C3AN00807J>.
- [98] F.S. Ruggeri, J. Habchi, S. Chia, R.I. Horne, M. Vendruscolo, T.P. Knowles, Infrared nanospectroscopy reveals the molecular interaction fingerprint of an aggregation inhibitor with single A β 42 oligomers, *Nat. Commun.* 12 (1) (2021) 688, <https://doi.org/10.1038/s41467-020-20782-0>.
- [99] T.O. Pavia, A. Schneider, L. Bataille, A. Chovin, A. Anne, T. Michon, C. Wege, C. Demaille, Enzymatic activity of individual bioelectrocatalytic viral nanoparticles: dependence of catalysis on the viral scaffold and its length, *Nanoscale* 14 (875–889) (2022) 875–889, <https://doi.org/10.1039/d1nr07445h>.
- [100] M. Lanza, M.P.M. Nafria, X. Aymerich, E. Whittaker, B. Hamilton, Electrical resolution during conductive atomic force microscopy measurements under different environmental conditions and contact forces, *Rev. Sci. Instrum.* 81 (10) (2010), 106110, <https://doi.org/10.1063/1.3491956>.
- [101] J. Park, J. Yang, G. Lee, C.Y. Lee, S. Na, S.W. Lee, S. Haam, Y.-M. Huh, D.S. Yoon, K. Eom, T. Kwon, Single-molecule recognition of biomolecular interaction via Kelvin probe force microscopy, *ACS Nano* 5 (9) (2011) 6981–6990, <https://doi.org/10.1021/nn201540c>.
- [102] C. Marcuello, L. Chambel, M.S. Rodrigues, L.P. Ferreira, M.M. Cruz, Magnetotactic bacteria: magnetism beyond magnetosomes, *IEEE Trans. Nanobiosci.* 17 (4) (2018) 555–559, <https://doi.org/10.1109/TNB.2018.2878085>.
- [103] L. Li, P. Zhang, J. Li, Y. Wang, Y. Wei, J. Hu, X. Zhou, B. Xu, B. Li, Measurement of nanomechanical properties of DNA molecules by PeakForce atomic force microscopy based on DNA origami, *Nanoscale* 11 (11) (2019) 4707–4711, <https://doi.org/10.1039/c8nr10354b>.
- [104] D.J. Müller, A.C. Dumitru, C. Lo Giudice, H.E. Gaub, P. Hinterdorfer, G. Hummer, J.J. De Yoreo, Y.F. Dufrene, D. Alsteens, Atomic force microscopy-based force spectroscopy and multiparametric imaging of biomolecular and cellular systems, *Chem. Rev.* 121 (19) (2021) 11701–11725, <https://doi.org/10.1021/acs.chemrev.0c00617>.
- [105] D.L. Malotky, M.K. Chaudhury, Investigation of capillary forces using atomic force microscopy, *Langmuir* 17 (25) (2001) 7823–7829, <https://doi.org/10.1021/la0107796>.
- [106] S. Shi, T. Wu, P. Zheng, Direct measurements of the cobalt-thiolate bonds strength in rubredoxin by single-molecule force spectroscopy, *Chembiochem.* 23 (12) (2022), e202200165, <https://doi.org/10.1002/cbic.202200165>.
- [107] S. Shi, Z. Wang, Y. Deng, F. Tian, Q. Wu, P. Zheng, Combination of click chemistry and enzymatic ligation for stable and efficient protein immobilization for single-molecule force spectroscopy, *CCS Chem.* 4 (2) (2022) 598–604, [10.1039/c2cc36355c](https://doi.org/10.1039/c2cc36355c).
- [108] S. Cui, J. Yu, F. Kühner, K. Schulten, H.E. Gaub, Double-stranded DNA dissociates into single strands when dragged into a poor solvent, *J. Am. Chem. Soc.* 129 (47) (2007) 14710–14716, <https://doi.org/10.1021/ja074776c>.
- [109] H. Wang, Y. Chen, W. Zhang, A single-molecule atomic force microscopy study reveals the antiviral mechanism of tannin and its derivatives, *Nanoscale* 11 (35) (2019) 16368–16376, <https://doi.org/10.1039/c9nr05410c>.
- [110] H. Grubmüller, B. Heymann, P. Tavan, Ligand binding: molecular mechanics calculation of the streptavidin-biotin rupture force, *Science* 271 (5251) (1996) 997–999, <https://doi.org/10.1126/science.271.5251.997>.
- [111] P. Hinterdorfer, W. Baumgartner, H.J. Gruber, K. Schilcher, H. Schindler, Detection and localization of individual antibody-antigen recognition events by atomic force microscopy, *Proc. Natl. Acad. Sci. U. S. A.* 93 (8) (1996) 3477–3488, <https://doi.org/10.1073/pnas.93.8.3477>.
- [112] H.-J. Butt, B. Cappella, M. Kappl, Force measurements with the atomic force microscope: technique, interpretation and applications, *Surf. Sci. Rep.* 59 (1–6) (2005) 1–152, <https://doi.org/10.1016/j.surfrep.2005.08.003>.
- [113] M. Boudaoud, Y. Haddab, Y. Le Gorrec, P. Lutz, Study of thermal and acoustic noise interferences in low stiffness atomic force microscope cantilevers and characterization of their dynamic properties, *Rev. Sci. Instrum.* 83 (1) (2012), 013704, <https://doi.org/10.1063/1.3673637>.
- [114] A.D.L. Humphris, J. Tamayo, J. Miles, Active quality factor control in liquids for force spectroscopy, *Langmuir* 16 (2000) 7891–7894, <https://doi.org/10.1021/la000766c>.
- [115] J.L. Hutter, J. Bechhoefer, Calibration of atomic-force microscope tips, *Rev. Sci. Instrum.* 64 (1993) 1868, <https://doi.org/10.1063/1.1143970>.
- [116] J.E. Sader, Method for the calibration of atomic force microscope cantilevers, *Rev. Sci. Instrum.* 66 (1995) 3789, <https://doi.org/10.1063/1.1154339>.
- [117] H. Schillers, C. Rianna, J. Schüppe, T. Luque, H. Döschke, M. Wälter, J.J. Uriarte, N. Campillo, G.P.A. Michanetzis, J. Bobrowska, et al., Standardized nanomechanical atomic force microscopy procedure (SNAP) for measuring soft and biological samples, *Sci. Rep.* 7 (2017) 5117, <https://doi.org/10.1038/s41598-017-05383-0>.
- [118] J.R. Rodrigues, A. Gusso, F.S.S. Rosa, V.R. Almeida, Rigorous analysis of Casimir and van der Waals forces on a silicon nano-optomechanical device actuated by optical forces, *Nanoscale* 10 (8) (2018) 3945–3952, <https://doi.org/10.1039/c7nr09318g>.
- [119] J.-J. Wu, The jump-to-contact distance in atomic force microscopy measurement, *J. Adhes.* 86 (11) (2010) 1071–1085, <https://doi.org/10.1080/00218464.2010.519256>.
- [120] S. Cazaux, A. Sadoun, M. Biarnes-Pelicot, M. Martínez, S. Obeid, P. Bongrand, L. Limozin, P.-H. Puech, Synchronizing atomic force microscopy force mode and fluorescence microscopy in real time for immune cell stimulation and activation studies, *Ultramicroscopy* 160 (2016) 168–181, <https://doi.org/10.1016/j.ultramicro.2015.10.014>.
- [121] H.A. Kramers, Brownian motion in a field of force and the diffusion model of chemical reactions, *Physica* 7 (4) (1940) 284–304, [https://doi.org/10.1016/S0031-8914\(40\)90098-2](https://doi.org/10.1016/S0031-8914(40)90098-2).
- [122] C. Bouchiat, M.D. Wang, J. Allemand, T. Strick, S.M. Block, V. Croquette, Estimating the persistence length of a worm-like chain molecule from force-extension measurements, *Biophys. J.* 76 (1 Pt1) (1999) 409–413, [https://doi.org/10.1016/s0006-3495\(99\)77207-3](https://doi.org/10.1016/s0006-3495(99)77207-3).
- [123] B. Freund, Characterizing the resistance generated by a molecular bond as it is forcibly separated, *Proc. Natl. Acad. Sci. U. S. A.* 106 (22) (2009) 8818–8823, <https://doi.org/10.1073/pnas.0903003106>.
- [124] J. Zlatanova, S.M. Lindsay, S.H. Leuba, Single molecule force spectroscopy in biology using the atomic force microscope, *Prog. Biophys. Mol. Biol.* 74 (1–2) (2000) 37–61, [https://doi.org/10.1016/S0079-6107\(00\)00014-6](https://doi.org/10.1016/S0079-6107(00)00014-6).
- [125] A.S. Lea, A. Pungor, V. Hlady, J.D. Andrade, J.N. Herron, E.W. Voss, Manipulation of proteins on mica by atomic force microscopy, *Langmuir* 8 (1) (1992) 68–73, <https://doi.org/10.1021/la00037a015>.
- [126] P.G. Georgiou, A.N. Baker, S.-J. Richards, A. Laezza, M. Walker, M.I. Gibson, Tuning aggregative versus non-aggregative lectin binding with glycosylated nanoparticles by the nature of the polymer ligand, *J. Mater. Chem. B* 8 (2020) 136–145, <https://doi.org/10.1039/c9tb02004g>.
- [127] C. Contini, J.W. Hindley, T.J. Macdonald, J.D. Barritt, O. Ces, N. Quirke, Size dependency of gold nanoparticles interacting with model membranes, *Commun. Chem.* 3 (1) (2020) 130, <https://doi.org/10.1038/s42004-020-00377-y>.
- [128] E. Cruz, V. Kayser, Synthesis and enhanced cellular uptake in vitro of anti-HER2 multifunctional gold nanoparticles, *Cancers* 11 (6) (2019) 870, <https://doi.org/10.3390/cancers11060870>.
- [129] Z. Su, H. Xu, X. Xu, Y. Zhang, Y. Ma, C. Li, Q. Xie, Effective covalent immobilization of quinone and aptamer onto a gold electrode via thiol addition for sensitive and selective protein biosensing, *Talanta* 164 (2017) 244–248, <https://doi.org/10.1016/j.talanta.2016.11.049>.
- [130] M. Hen, M. Ronen, A. Deitch, E. Barbiro-Michaely, Z. Oren, C.N. Sukenik, D. Gerber, An off-the-shelf integrated microfluidic device comprising self-assembled monolayers for protein array experiments, *Biomicrofluidics* 9 (5) (2015), 054108, <https://doi.org/10.1063/1.4930982>.
- [131] U. Maver, O. Planinsek, J. Kamnik, A.I. Hassanien, M. Gaberscek, Preparation of atomically flat gold substrates for AFM measurements, *Acta Chim. Slov.* 59 (1) (2012) 212–219.
- [132] E.V. Dubrovin, M. Schächtele, D.V. Klinov, T.E. Schäffer, Time-lapse single-molecule atomic force microscopy investigation on modified graphite in solution, *Langmuir* 33 (38) (2017) 10027–10034, <https://doi.org/10.1021/acs.langmuir.7b02220>.
- [133] Y. Li, N. Li, L. Wang, Q. Lu, X. Ji, F. Zhang, A comparative study on the self-assembly of peptide TGV-9 by in situ atomic force microscopy, *Micros. Microanal.* 26 (2) (2020) 319–325, <https://doi.org/10.1017/S1431927620000082>.
- [134] F. Kienberger, V.P. Pastushenko, G. Kada, H.J. Gruber, C. Riener, H. Schindler, P. Hinterdorfer, Static and dynamical properties of single poly(ethylene glycol) molecules investigated by force spectroscopy, *Single Mol.* 1 (2) (2000) 123–128, [https://doi.org/10.1002/1438-5171\(200006\)1:2<123::AID-SIMO123>3.0.CO;2-3](https://doi.org/10.1002/1438-5171(200006)1:2<123::AID-SIMO123>3.0.CO;2-3).
- [135] J. Sotres, A. Lostao, L. Wildling, A. Ebner, C. Gómez-Moreno, H.J. Gruber, P. Hinterdorfer, A.M. Baró, Unbinding molecular recognition force maps of localized single receptor molecules by atomic force microscopy, *ChemPhysChem* 9 (4) (2008) 590–599, <https://doi.org/10.1002/cphc.200700597>.
- [136] C. Marcuello, R. de Miguel, C. Gómez-Moreno, M. Martínez-Júlvez, A. Lostao, An efficient method for enzyme immobilization evidenced by atomic force microscopy, *Protein Eng. Des. Sel.* 25 (11) (2012) 715–723, <https://doi.org/10.1093/protein/gzs086>.
- [137] E. Makou, R.G. Bailey, H. Johnston, J.D. Parkin, A.N. Hulme, G. Hähner, P. N. Barlow, Combining SPR with atomic-force microscopy enables single-molecule insights into activation and suppression of the complement cascade, *J. Biol. Chem.* 294 (52) (2019) 20148–20163, <https://doi.org/10.1074/jbc.RA119.010913>.
- [138] B. Wang, B. Park, B. Xu, Y. Kwon, Label-free biosensing of *Salmonella enterica* serovars at single-cell level, *J. Nanobiotechnol.* 15 (1) (2017) 40, <https://doi.org/10.1186/s12591-017-0273-6>.
- [139] E. Suleiman, J. Mayer, E. Lehner, B. Kohlhauser, A. Katholnig, M. Batzoni, D. Damm, V. Temchura, A. Wagner, K. Überla, et al., Conjugation of native-like HIV-1 envelope trimers onto liposomes using EDC/sulfo-NHS chemistry: requirements and limitations, *Pharmaceutics* 12 (10) (2020) 979, <https://doi.org/10.3390/pharmaceutics12100979>.
- [140] D. Kamsma, P. Bochet, F. Oswald, N. Alblas, S. Goyard, G.J.L. Wuite, E.J. G. Peterman, T. Rose, Single-cell acoustic force spectroscopy: resolving kinetics

- and strength of T cell adhesion to fibronectin, *Cell Rep.* 24 (11) (2018) 3008–3016, <https://doi.org/10.1016/j.celrep.2018.08.034>.
- [141] M.P. Wickramathilaka, B.Y. Tao, Characterization of covalent crosslinking strategies for synthesizing DNA-based bioconjugates, *J. Biol. Eng.* 13 (2019) 63, <https://doi.org/10.1186/s13036-019-0191-2>.
- [142] D. Mitchell III, A.J. Renda, C.A. Douds, P. Babitzke, S.M. Assmann, P. C. Bevilacqua, In vivo RNA structural probing of uracil and guanine base-pairing by 1-ethyl-3-(3-dimethylaminopropyl)carbodiimide (EDC), *RNA* 25 (1) (2019) 147–157, <https://doi.org/10.1261/ma.067868.118>.
- [143] X. Shi, Y. Jung, L.-J. Lin, C. Liu, C. Wu, I.K.O. Cann, T. Ha, Quantitative fluorescence labeling of aldehyde-tagged proteins for single-molecule imaging, *Nat. Methods* 9 (2012) 499–503, <https://doi.org/10.1038/nmeth.1954>.
- [144] M. Sorci, B. Dassa, H. Liu, G. Anand, A.K. Dutta, S. Pietrokovski, M. Belfort, G. Belfort, Oriented covalent immobilization of antibodies for measurement of intermolecular binding forces between zipper-like contact surfaces of split inteins, *Anal. Chem.* 85 (12) (2013) 6080–6088, <https://doi.org/10.1021/ac400949t>.
- [145] R. Walder, M.-A. LeBlanc, W.J. Van Patten, D.T. Edwards, J.A. Greenberg, A. Adhikari, S.R. Okoniewski, R.M.A. Sullan, D. Rabuka, M.C. Sousa, et al., Rapid characterization of a mechanically labile α -helical protein enabled by efficient site-specific bioconjugation, *J. Am. Chem. Soc.* 139 (29) (2017) 9867–9875, <https://doi.org/10.1021/jacs.7b02958>.
- [146] J.E.G. McCarthy, S. Marsden, T. von der Haar, Biophysical studies of the translation initiation pathway with immobilized mRNA analogs, *Methods Enzymol.* 430 (2007) 247–264, [https://doi.org/10.1016/S0076-6879\(07\)30010-4](https://doi.org/10.1016/S0076-6879(07)30010-4).
- [147] J. Popplewell, M. Swann, G. Brown, B. Lauder, Fabrication of carbohydrate surfaces by using non-derivatised oligosaccharides, *Methods Mol. Biol.* 808 (2012) 221–229, https://doi.org/10.1007/978-1-61779-373-8_15.
- [148] Q. Wu, W. Dong, H. Miao, Q. Wang, S. Dong, W. Xuan, Site-specific protein modification with reducing carbohydrates, *Angew. Chem. Int. Ed. Engl.* 61 (19) (2022), e202116545, <https://doi.org/10.1002/anie.202116545>.
- [149] C. Marcuello, R. de Miguel, M. Martínez-Júlviz, C. Gómez-Moreno, A. Lostao, Mechanostability of the single-electron-transfer complexes of anaerobic ferredoxin-NADP(+) reductase, *ChemPhysChem* 16 (15) (2015) 3161–3169, <https://doi.org/10.1002/cphc.201500534>.
- [150] C. Marcuello, R. de Miguel, A. Lostao, Molecular recognition of proteins through quantitative force maps at single molecule level, *Biomolecules* 12 (4) (2022) 594, <https://doi.org/10.3390/biom12040594>.
- [151] K.H. Hu, M.J. Butte, T cell activation requires force generation, *J. Cell Biol.* 213 (5) (2016) 535–542, <https://doi.org/10.3390/molecules25235672>.
- [152] S. Pérez-Domínguez, S. Caballero-Mancebo, C. Marcuello, M. Martínez-Júlviz, M. Medina, A. Lostao, Nanomechanical study of enzyme: coenzyme complexes: bipartite sites in plastidic ferredoxin-NADP+ reductase for the interaction with NADP, *Antioxidants* 11 (3) (2022) 537, <https://doi.org/10.3390/antiox11030537>.
- [153] B. Almeida, O.K. Nag, K.E. Rogers, J.B. Delehanty, Recent progress in bioconjugation strategies for liposome-mediated drug delivery, *Molecules* 25 (23) (2020) 672, <https://doi.org/10.3390/molecules25236672>.
- [154] I. Jasim, Z. Shen, Z. Mlaji, N.S. Yuksek, A. Abdullah, J. Liu, S.G. Dastider, M. El-Dweik, S. Zhang, M. Almasri, An impedance biosensor for simultaneous detection of low concentration of Salmonella serogroups in poultry and fresh produce samples, *Biosens. Bioelectron.* 126 (2019) 292–300, <https://doi.org/10.1016/j.bios.2018.10.065>.
- [155] S. Lee, S. Park, M.T. Nguyen, E. Lee, L. Kim, S. Baek, C.J. Kim, Y.J. Jang, H. A. Choe, A chemical conjugate between HER2-targeting antibody fragment and Pseudomonas exotoxin A fragment demonstrates cytotoxic effects on HER2-expressing breast cancer cells, *BMB Rep.* 52 (8) (2019) 496–501, <https://doi.org/10.5483/BMBRep.2019.52.8.250>.
- [156] J. Lin, Y. Hu, J.-J. Zhao, Repression of multiple myeloma cell growth in vivo by single-wall carbon nanotube (SWCNT)-delivered MALAT1 antisense oligos, *J. Vis. Exp.* 142 (2018), <https://doi.org/10.3791/58598>.
- [157] C. Marcuello, L. Foulon, B. Chabbert, M. Molinari, V. Aguié-Béguin, Langmuir-Blodgett procedure to precisely control the coverage of functionalized AFM cantilevers for SMFS measurements: application with cellulose nanocrystals, *Langmuir* 34 (32) (2018) 9376–9386, <https://doi.org/10.1021/acs.langmuir.8b01892>.
- [158] C. Marcuello, L. Foulon, B. Chabbert, V. Aguié-Béguin, M. Molinari, Atomic force microscopy reveals how relative humidity impacts the Young's modulus of lignocellulosic polymers and their adhesion with cellulose nanocrystals at the nanoscale, *Int. J. Biol. Macromol.* 147 (2020) 1064–1075, <https://doi.org/10.1016/j.ijbiomac.2019.10.074>.
- [159] F. Berzin, L. Lemkhanter, C. Marcuello, B. Chabbert, V. Aguié-Béguin, M. Molinari, R. Castellani, B. Vergnes, Influence of the polarity of the matrix on the breakage mechanisms of lignocellulosic fibers during twin-screw extrusion, *Polym. Compos.* 41 (3) (2020) 1106–1117, <https://doi.org/10.1002/pc.25442>.
- [160] E. Gerbin, Y.-M. Frapart, C. Marcuello, B. Cottyn, L. Foulon, M. Pernes, D. Crônier, M. Molinari, B. Chabbert, P.-H. Ducrot, et al., Dual antioxidant properties and organic radical stabilization in cellulose nanocomposite films functionalized by in situ polymerization of coniferyl alcohol, *Biomacromolecules* 21 (8) (2020) 3163–3175, <https://doi.org/10.1021/acs.biomac.0c00583>.
- [161] E. Gerbin, G.N. Rivière, L. Foulon, Y.M. Frapart, B. Cottyn, M. Pernes, C. Marcuello, B. Godon, A. Gainvors-Claisse, D. Crônier, et al., Tuning the functional properties of lignocellulosic films by controlling the molecular and supramolecular structure of lignin, *Int. J. Biol. Macromol.* 181 (2021) 136–149, <https://doi.org/10.1016/j.ijbiomac.2021.03.081>.
- [162] D. Corregidor, R. Tabraue, L. Colchero, R. Daza, M. Elices, G.V. Guinea, J. Pérez-Rigueiro, High-yield characterization of single molecule interactions with DeepTip™ atomic force microscopy probes, *Molecules* 28 (1) (2022) 226, <https://doi.org/10.3390/molecules28010226>.
- [163] M. Koehler, C. Lo Giudice, P. Vogl, A. Ebner, P. Hinterdorfer, H.J. Gruber, D. Alsteens, Control of ligand-binding specificity using photocleavable linkers in AFM force spectroscopy, *Nano Lett.* 20 (5) (2020) 4038–4042, <https://doi.org/10.1021/acs.nanolett.0c01426>.
- [164] R.-X. Yao, J.-J. Shei, K.-H. Li, X. Liu, H.-Y. Zhang, M. Wang, W.-K. Zhang, Exploring the nanomechanical properties of a coordination-bond based supramolecular polymer, *Chin. J. Polym. Sci.* 40 (2022) 1613–1622, <https://doi.org/10.1007/s10118-022-2797-y>.
- [165] L.F. Milles, K. Schulten, H.E. Gaub, R.C. Bernardi, Molecular mechanism of extreme mechanostability in a pathogen adhesion, *Science* 359 (6383) (2018) 1527–1533, <https://doi.org/10.1126/science.aar2094>.
- [166] C. He, G.Z. Genchev, H. Lu, H. Li, Mechanically untying a protein slipknot: multiple pathways revealed by force spectroscopy and steered molecular dynamics simulations, *J. Am. Chem. Soc.* 134 (25) (2012) 10428–10435, <https://doi.org/10.1021/ja3003205>.
- [167] G.I. Bell, Models for the specific adhesion of cells to cells: a theoretical framework for adhesion mediated by reversible bonds between cell surface molecules, *Science* 200 (4342) (1978) 618–627, <https://doi.org/10.1126/science.347575>.
- [168] E. Evans, K. Ritchie, Dynamic strength of molecular adhesion bonds, *Biophys. J.* 72 (4) (1997) 1541–1555, [https://doi.org/10.1016/S0006-3495\(97\)78802-7](https://doi.org/10.1016/S0006-3495(97)78802-7).
- [169] R. Merkel, P. Nassoy, A. Leung, K. Ritchie, E. Evans, Energy landscapes of receptor-ligand bonds explored with dynamic force spectroscopy, *Nature* 397 (6714) (1999) 50–53, <https://doi.org/10.1038/16219>.
- [170] C.-K. Lee, Y.-M. Wang, L.-S. Huang, S. Lin, Atomic force microscopy: determination of unbinding force, off rate and energy barrier for protein-ligand interaction, *Micron* 38 (5) (2007) 446–461, <https://doi.org/10.1016/j.micron.2006.06.014>.
- [171] F.T. Hane, R. Hayes, B.Y. Lee, Z. Leonenko, Effect of copper and zinc on the single molecule self-affinity of Alzheimer's amyloid- β peptides, *PLoS One* 11 (1) (2016), e0147488, <https://doi.org/10.1371/journal.pone.0147488>.
- [172] A. Harder, V. Walhorn, T. Dierks, X. Fernández-Busquets, D. Anselmetti, Single-molecule force spectroscopy of cartilage aggrecan self-adhesion, *Biophys. J.* 99 (10) (2010) 3498–3504, <https://doi.org/10.1016/j.bpj.2010.09.002>.
- [173] S. Li, X. Pang, J. Zhao, Q. Zhang, Y. Shan, Evaluation the single-molecule interactions between targeted peptides and the receptors on living cell membrane, *Nanoscale* 13 (2021) 17318–17324, <https://doi.org/10.1039/D1NR05547J>.
- [174] C.P.A. Doherty, L.M. Young, T.K. Karamanos, H.I. Smith, M.P. Jackson, S. E. Radford, D.J.A. Brockwell, A peptide-display protein scaffold to facilitate single molecule force studies of aggregation-prone peptides, *Protein Sci.* 27 (7) (2018) 1205–1217, <https://doi.org/10.1002/pro.3386>.
- [175] A. Berquand, N. Xia, D.G. Castner, B.H. Clare, N.L. Abbott, V. Dupres, Y. Adriaenssen, Y.F. Dufrene, Antigen binding forces of single antilysozyme Fv fragments explored by atomic force microscopy, *Langmuir* 21 (12) (2005) 5517–5523, <https://doi.org/10.1021/la050162e>.
- [176] J.-M. Teulon, Y. Delcuze, M. Odorico, S.-W.W. Chen, P. Parot, J.-L. Pellequer, Single and multiple bonds in (strept)avidin-biotin interactions, *J. Mol. Recognit.* 24 (3) (2011) 490–502, <https://doi.org/10.1002/jmr.1109>.
- [177] E. Sengupta, Y. Yan, X. Wang, K. Munechika, D.S. Ginger, Dynamic force spectroscopy of photoswitch-modified DNA, *ACS Nano* 8 (3) (2014) 2625–2631, <https://doi.org/10.1021/nn406334b>.
- [178] B. Bonnani, A.S.M. Kamruzzahan, A.R. Bizarri, C. Rankl, H.J. Bruber, P. Hinterdorfer, S. Cannistraro, Single molecule recognition between cytochrome C 551 and gold-immobilized azuring by force spectroscopy, *Biophys. J.* 89 (4) (2005) 2783–2791, <https://doi.org/10.1529/biophysj.105.064097>.
- [179] M. Goktas, C. Luo, R.M.A. Sullan, A.E. Bergues-Pupo, R. Lipowsky, A.V. Verde, K. G. Blank, Molecular mechanics of coiled coils loaded in the shear geometry, *Chem. Sci.* 9 (2018) 4610–4621, <https://doi.org/10.1039/C8SC01037D>.
- [180] O.E. Farrance, E. Hann, R. Kaminska, N.G. Housden, S.R. Derrington, C. Kleanthous, S.E. Radford, D.J. Brockwell, A force-activated trip switch triggers rapid dissociation of a colicin from its immunity protein, *PLoS Biol.* 11 (2) (2013), e1001489, <https://doi.org/10.1371/journal.pbio.1001489>.
- [181] K. Lebed, A.J. Kulik, L. Forró, M. Lekka, Atomic force microscopy and quartz crystal microbalance study of the lectin-carbohydrate interaction kinetics, *Acta Phys. Pol. A* 111 (2) (2007) 273–286, <https://doi.org/10.12693/APhysPolA.111.273>.
- [182] A. Burmistrova, B. Fresch, D. Sluysmans, E. De Pauw, F. Remacle, A.-S. Duwez, Force measurements reveal how small binders perturb the dissociation mechanisms of DNA complex sequences, *Nanoscale* 8 (2016) 11718–11726, <https://doi.org/10.1039/c6nr02201d>.
- [183] W. Baumgartner, P. Hinterdorfer, W. Ness, A. Raab, D. Vestweber, H. Schindler, D. Drenckhahn, Cadherin interaction probed by atomic force microscopy, *Proc. Natl. Acad. Sci. U. S. A.* 97 (8) (2000) 4005–4010, <https://doi.org/10.1073/pnas.070052697>.
- [184] S. Lynch, H. Baker, S.G. Byker, D. Zhou, K. Sinniah, Single molecule force spectroscopy on G-quadruplex DNA, *Chemistry* 15 (33) (2009) 8113–8116, <https://doi.org/10.1002/chem.200901390>.
- [185] V. Reiter-Scherer, J.L. Cuellar-Camacho, S. Bhatia, R. Haag, A. Herrmann, D. Lauster, J.P. Rabe, Force spectroscopy shows dynamic binding of influenza hemagglutinin and neuraminidase to sialic acid, *Biophys. J.* 116 (6) (2019) 1577, <https://doi.org/10.1016/j.bpj.2019.03.032>.
- [186] Y. Fu, J. Wang, Y. Wang, H. Sun, Investigating the effect of tyrosine kinase inhibitors on the interaction between human serum albumin by atomic force

- microscopy, *Biomolecules* 12 (2022) 819, <https://doi.org/10.3390/biom12060819>.
- [187] W. Dettmann, M. Grandbois, S. André, M. Benoit, A.K. Wehle, H. Kaltner, H. J. Gabius, H.E. Gaub, Differences in zero-force and force-driven kinetics of ligand dissociation from beta-galactoside-specific proteins (plant and animal lectins, immunoglobulin G) monitored by plasmon resonance and dynamic single molecule force spectroscopy, *Arch. Biochem. Biophys.* 383 (2000) 157–170, <https://doi.org/10.1006/abbi.2000.1993>.
- [188] M. Sletmoen, T.K. Dam, T.A. Gerken, B.T. Stokke, C.F. Brewer, Single-molecule pair studies of the interactions of the alpha-GalNAc (Tn-antigen) form of porcine submaxillary mucin with soybean agglutinin, *Biopolymers* 91 (9) (2009) 719–728, <https://doi.org/10.1002/bip.21213>.
- [189] V. Botti, S. Marrone, S. Cannistraro, A.R. Bizarri, Interaction between miR4729 and human serum albumin as revealed by fluorescence, FRET, atomic force spectroscopy and computational modelling, *Int. J. Mol. Sci.* 23 (3) (2022) 291, <https://doi.org/10.3390/ijms23031291>.
- [190] D. Sluysmans, F. Devaux, C.J. Bruns, J.F. Stoddart, A.-S. Duwez, Dynamic force spectroscopy of synthetic oligorotaxane foldamers, *Proc. Natl. Acad. Sci. U. S. A.* 115 (38) (2018) 9362–9366, <https://doi.org/10.1073/pnas.1712790115>.
- [191] M. Taranta, A.R. Bizarri, S. Cannistraro, Probing the interaction between p53 and the bacterial protein azurin by single molecule force spectroscopy, *J. Mol. Recognit.* 21 (1) (2008) 63–70, <https://doi.org/10.1002/jmr.869>.
- [192] T. Maki, S. Kidoaki, K. Usui, H. Suzuki, M. Ito, F. Ito, Y. Hayashizaki, T. Matsuda, Dynamic force spectroscopy of the specific interaction between the PDZ domain and its recognition peptides, *Langmuir* 23 (5) (2007) 2668–2673, <https://doi.org/10.1021/la0627011>.
- [193] G. Andre, K. Leenhouts, P. Hols, Y.F. Dufrene, Detection and localization of single LysM-peptidoglycan interactions, *J. Bacteriol.* 190 (21) (2008) 7079–7086, <https://doi.org/10.1128/JB.00519-08>.
- [194] N.H. Green, P.M. Williams, O. Wahab, M.C. Davies, C.J. Roberts, S.J.B. Tendler, S. Allen, Single-molecule investigations of RNA dissociation, *Biophys. J.* 86 (6) (2004) 3811–3821, <https://doi.org/10.1529/biophysj.103.026070>.
- [195] M. de Odrowaz Piramowicz, P. Czuba, M. Targosz, K. Burda, M. Szymonski, Dynamic force measurements of avidin-biotin and streptavidin-biotin interactions using AFM, *Acta Biochim. Pol.* 53 (1) (2006) 93–100, [10.18388/abp.2006.3367](https://doi.org/10.18388/abp.2006.3367).
- [196] Y. Gilbert, M. Deghorain, L. Wang, B. Xu, P.D. Pollheimer, H.J. Gruber, J. Errington, B. Hallet, X. Haulot, C. Verbeelen, et al., Single-molecule force spectroscopy and imaging of the Vancomycin-D-ala-D-ala interaction, *Nano Lett.* 7 (3) (2007) 796–801, <https://doi.org/10.1021/nl0700853>.
- [197] S. Posch, C. Aponte-Santamaria, R. Schwarzl, A. Karner, M. Radtke, F. Gräter, T. Obser, G. König, M.A. Brehm, H.J. Gruber, et al., Single molecule force spectroscopy data and BD-MD simulations on the blood protein von Willebrand factor, *Data Brief* 8 (2016) 1080–1087, <https://doi.org/10.1016/j.dib.2016.07.031>.
- [198] A. Ptak, M. Makowski, M. Cichomski, Characterization of nanoscale adhesion between a fluoroalkyl silane monolayer and a silicon AFM tip. Complex character of the interaction potential, *Chem. Phys. Lett.* 489 (1–3) (2010) 54–58, <https://doi.org/10.1016/j.cplett.2010.02.043>.
- [199] K. Herman, M. Lekka, A. Ptak, Unbinding kinetics of syndecans by single-molecule force spectroscopy, *J. Phys. Chem. Lett.* 9 (7) (2018) 1509–1515, <https://doi.org/10.1021/acs.jpclett.7b03420>.
- [200] M. Lekka, K. Herman, J. Zemla, L. Bodek, G. Pyka-Fościk, D. Gil, J. Dulińska-Litewka, A. Ptak, P. Laidler, Probing the recognition specificity of α v β 1 integrin and syndecan-4 using force spectroscopy, *Micron* 37 (2020), 102888, <https://doi.org/10.1016/j.micron.2020.102888>.
- [201] O.K. Dudko, G. Hummer, A. Szabo, Intrinsic rates and activation free energies from single-molecule pulling experiments, *Phys. Rev. Lett.* 96 (10) (2006), 108101, <https://doi.org/10.1103/PhysRevLett.96.108101>.
- [202] G.G. Hummer, A. Szabo, Kinetics from nonequilibrium single-molecule pulling experiments, *Biophys. J.* 85 (1) (2003) 5–15, [https://doi.org/10.1016/S0006-3495\(03\)74449-X](https://doi.org/10.1016/S0006-3495(03)74449-X).
- [203] O.K. Dudko, A.E. Filipov, J. Klafter, M. Urbakh, Beyond the conventional description of dynamic force spectroscopy of adhesion bonds, *Proc. Natl. Acad. Sci. U. S. A.* 100 (20) (2003) 11378–11381, <https://doi.org/10.1073/pnas.1534554100>.
- [204] R. Tapia-Rojas, C. Marcuello, A. Lostao, C. Gómez-Moreno, J.J. Mazo, F. Falo, A physical picture for mechanical dissociation of biological complexes: from forces to free energies, *Phys. Chem. Chem. Phys.* 19 (2017) 4567–4575, <https://doi.org/10.1039/c6cp07508h>.
- [205] F. Rico, L. Gonzalez, I. Casuso, M. Puig-Vidal, S. Scheuring, High-speed force spectroscopy unfolds titin at the velocity of molecular dynamic simulations, *Science* 342 (6159) (2013) 741–743, <https://doi.org/10.1126/science.1239764>.
- [206] K. Herman, M. Weiss, M. Lekka, A. Ptak, How complex is the concanavalin A-carboxypeptidase Y interaction? *ACS Chem. Biol.* 14 (7) (2019) 1611–1618, <https://doi.org/10.1021/acscchembio.9b00337>.
- [207] J. Dąbrowski, W. Nowak, A. Ptak, Enthalpic and entropic contributions to the activation free energy of single noncovalent bonds in molecular systems: a computational methodology, *Phys. Rev. A* 106 (2022), 062803, <https://doi.org/10.1103/PhysRevA.106.062803>.
- [208] R.W. Friddle, A. Noy, J.J. De Yoreo, Interpreting the widespread nonlinear force spectra of intermolecular bonds, *Proc. Natl. Acad. Sci. U.S.A.* 109 (34) (2012) 13573–13578, <https://doi.org/10.1073/pnas.1202946109>.
- [209] F.T. Hane, S.J. Attwood, Z. Leonenko, Comparison of three competing dynamic force spectroscopy models to study binding forces of amyloid- β (1–42), *Soft Matter* 10 (12) (2014) 1924–1930, <https://doi.org/10.1039/c3sm52257a>.
- [210] J. Dąbrowski, W. Nowak, A. Ptak, How strong are hydrogen bonds in the peptide model? *Phys. Chem. Chem. Phys.* 22 (2020) 1392–1399, <https://doi.org/10.1039/C9CP05564A>.
- [211] A. Ptak, M. Kappl, H.-J. Butt, Modified atomic force microscope for high-rate dynamic force spectroscopy, *Appl. Phys. Lett.* 88 (26) (2006), 263109, <https://doi.org/10.1063/1.2218273>.
- [212] I. Casuso, L. Redondo-Morata, F. Rico, Biological physics by high-speed atomic force microscopy, *Philos. Trans. A Math. Phys. Eng. Sci.* 378 (2020), 20190604, <https://doi.org/10.1098/rsta.2019.0604>.
- [213] C. Jarzynski, Nonequilibrium equality for free energy differences, *Phys. Rev. Lett.* 78 (1997) 2690, <https://doi.org/10.1103/PhysRevLett.78.2690>.
- [214] N.C. Harris, Y. Song, C.-H. Kiang, Experimental free energy surface reconstruction from single-molecule force spectroscopy using Jarzynski's equality, *Phys. Rev. Lett.* 99 (6) (2007), 068101, <https://doi.org/10.1103/PhysRevLett.99.068101>.
- [215] C.M. Stroh, A. Ebner, M. Geretschlager, G. Freudenthal, F. Kienberger, A.S. M. Kamruzzahan, S.J. Smith-Gill, H.J. Gruber, P. Hinterdofer, Simultaneous topography and recognition imaging using force microscopy, *Biophys. J.* 87 (3) (2004) 1981–1990, <https://doi.org/10.1529/biophysj.104.043331>.
- [216] M. Hofer, S. Adamsmaier, T.S. van Zanten, L.A. Chtcheglova, C. Manzo, M. Duman, B. Mayer, A. Ebner, M. Moerdelmaier, G. Kada, et al., Molecular recognition imaging using tuning-fork based transverse dynamic force microscopy, *Ultramicroscopy* 110 (6) (2010) 605–611, <https://doi.org/10.1016/j.ultramicro.2010.02.019>.
- [217] A. Ebner, F. Kienberger, G. Kada, C.M. Stroh, M. Geretschlager, A.S. M. Kamruzzahan, L. Wildling, W.T. Johnson, B. Ashcroft, J. Nelson, et al., Localization of single avidin-biotin interactions using simultaneous topography and molecular recognition imaging, *ChemPhysChem* 6 (5) (2005) 897–900, <https://doi.org/10.1002/cphc.200400545>.
- [218] L.A. Chtcheglova, F. Atalar, U. Ozbek, L. Wildling, A. Ebner, P. Hinterdofer, Localization of the ergotxin-1 receptors on the voltage sensing domain of hERG K + channel by AFM recognition imaging, *Pluggers Arch.* 456 (1) (2008) 247–254, <https://doi.org/10.1007/s00424-007-0418-9>.
- [219] R. Creasey, S. Sharma, J.E. Craig, C.T. Gibson, A. Ebner, P. Hinterdofer, N. H. Voelcker, Detecting protein aggregates on untreated human tissue samples by atomic force microscopy recognition imaging, *Biophys. J.* 99 (5) (2010) 1660–1667, <https://doi.org/10.1016/j.bpj.2010.06.044>.
- [220] M. Koehler, G. Macher, A. Rupperecht, R. Zhu, H.J. Gruber, E.E. Pohl, P. Hinterdofer, Combined recognition imaging and force spectroscopy: a new mode for mapping and studying interaction sites at low lateral density, *Sci. Adv. Mater.* 9 (1) (2017) 128–134, <https://doi.org/10.1166/sam.2017.3066>.
- [221] R. Garcia, Nanomechanical mapping of soft materials with the atomic force microscope: methods, theory and applications, *Chem. Soc. Rev.* 49 (2020) 5850–5884, <https://doi.org/10.1039/D0CS00318B>.
- [222] D. Lee, Y. Woo, J.-S. Lim, I. Park, S.K. Park, J.W. Park, Quantification of a neurological protein in a single cell without amplification, *ACS Omega* 7 (23) (2022) 20165–20171, <https://doi.org/10.1021/acsomega.2c02009>.
- [223] F. Moreno-Herrero, J. Colchero, J. Gómez-Herrero, A.M. Baró, Atomic force microscopy contact, tapping, and jumping modes for imaging biological samples in liquids, *Phys. Rev. E Stat. Nonlinear Soft Matter Phys.* 69 (3Pt1) (2004), 031915, <https://doi.org/10.1103/PhysRevE.69.031915>.
- [224] J. Sotres, A. Lostao, C. Gómez-Moreno, A.M. Baró, Jumping mode AFM imaging of biomolecules in the repulsive electrical double layer, *Ultramicroscopy* 107 (12) (2007) 1207–1212, <https://doi.org/10.1016/j.ultramicro.2007.01.020>.
- [225] P. Debye, E. Hückel, The theory of electrolytes. I. Lowering of freezing point and related phenomena, *Phys. Z.* 24 (1923) 185–206.
- [226] J.N. Israelachvili, G.E. Adams, Measurement of forces between two mica surfaces in aqueous electrolyte solutions in the range 0–100 nm, *J. Chem. Soc. Faraday Trans. 1* (74) (1978) 975–1001, <https://doi.org/10.1039/F19787400975>.
- [227] D. Derjaguin, L. Landau, Theory of the stability of strongly charged lyophobic sols and of the adhesion of strongly charged particles in solutions of electrolytes, *Proc. Acad. Sci. U.R.R.S.* 14 (1941) 633, [https://doi.org/10.1016/0079-6816\(93\)90013-L](https://doi.org/10.1016/0079-6816(93)90013-L).
- [228] E.J.W. Verwey, J.T.G. Overbeek, Theory of the stability of lyophobic colloids, *J. Phys. Colloid. Chem.* 51 (3) (1948) 631–636, <https://doi.org/10.1021/j150453a001>.
- [229] X. Shi, X. Fan, Y. Zhu, Y. Liu, P. Wu, R. Jiang, B. Wu, H.-A. Wu, H. Zheng, J. Wang, et al., Pushing detectability and sensitivity for subtle force to new limits with shrinkable nanochannel structured aerogel, *Nat. Commun.* 13 (1) (2022) 1119, <https://doi.org/10.1038/s41467-022-28760-4>.
- [230] F. Li, Y. Lin, A. Lau, Y. Tang, J. Chen, X.C. Le, Binding-induced molecular amplifier as a universal detection platform for biomolecules and biomolecular interaction, *Anal. Chem.* 90 (14) (2018) 8651–8657, <https://doi.org/10.1021/acs.analchem.8b01985>.
- [231] A. Quijano-Rubio, H.-W. Yeh, J. Park, H. Lee, R.A. Langan, S.E. Boyken, M. J. Lajoie, L. Cao, C.M. Chow, M.C. Miranda, et al., De novo design of modular and tunable protein biosensors, *Nature* 591 (7850) (2021) 482–487, <https://doi.org/10.1038/s41586-021-03258-z>.
- [232] P.B. Crowley, M. Ubbink, Close encounters of the transient kind: protein interactions in the photosynthetic redox chain investigated by NMR spectroscopy, *Acc. Chem. Res.* 36 (10) (2003) 723–730, <https://doi.org/10.1021/ar0200955>.
- [233] A. Yersin, T. Osada, A. Ikai, Exploring transferrin-receptor interactions at the single-molecule level, *Biophys. J.* 94 (1) (2008) 230–240, <https://doi.org/10.1529/biophysj.107.114637>.
- [234] L. Costa, M.S. Rodrigues, E. Newman, C. Zubieta, J. Chevrier, F. Comin, Imaging material properties of biological samples with a force feedback microscope, *J. Mol. Recognit.* 26 (12) (2013) 689–693, <https://doi.org/10.1002/jmr.2328>.

- [235] M.V. Vitorino, A. Viera, C.A. Marques, M.S. Rodrigues, Direct measurement of capillary condensation time of a water nanobridge, *Sci. Rep.* 8 (1) (2018) 13848, <https://doi.org/10.1038/s41598-018-32021-0>.
- [236] C. Marcuello, S. Arilla-Luna, M. Medina, A. Lostao, Detection of a quaternary organization into dimer of trimers of *Corynebacterium ammoniagenes* FAD synthetase at the single-molecule level and at the in cell level, *Biochim. Biophys. Acta* 1834 (3) (2013) 665–676, <https://doi.org/10.1016/j.bbapap.2012.12.013>.
- [237] R.A. Zamora, M. López-Ortiz, M. Sales-Mateo, C. Hu, R. Croce, R.A. Maniyara, V. Pruneri, M.I. Giannotti, P. Gorostiza, Light- and redox-dependent force spectroscopy reveals that the interaction between plastocyanin and plant photosystem I is favored when one partner is ready for electron transfer, *ACS Nano* 16 (9) (2022) 15155–15164, <https://doi.org/10.1021/acs.nano.2c06454>.
- [238] A. Rigato, A. Miyagi, S. Scheuring, F. Rico, High-frequency microrheology reveals cytoskeleton dynamics in living cells, *Nat. Phys.* 13 (8) (2017) 771–775, <https://doi.org/10.1038/nphys4104>.
- [239] M. Shimizu, C. Okamoto, K. Umeda, S. Watanabe, T. Ando, N. Kodera, An ultrafast piezoelectric Z-scanner with a resonance frequency above 1.1 MHz for high-speed atomic force microscopy, *Rev. Sci. Instrum.* 93 (1) (2022), 013701, <https://doi.org/10.1063/5.0072722>.
- [240] T. Ando, N. Kodera, E. Takai, D. Maruyama, K. Saito, A. Toda, A high-speed atomic force microscope for studying biological macromolecules, *Proc. Natl. Acad. Sci. U. S. A.* 98 (22) (2001) 12468–12472, <https://doi.org/10.1073/pnas.211400898>.
- [241] T. Ando, High-speed atomic force microscopy and its future prospects, *Biophys. Rev.* 10 (2) (2018) 285–292, <https://doi.org/10.1007/s12551-017-0356-5>.
- [242] C. Valotteau, F. Sumbul, F. Rico, High-speed force spectroscopy: microsecond force measurements using ultrashort cantilevers, *Biophys. Rev.* 11 (5) (2019) 689–699, <https://doi.org/10.1007/s12551-019-00585-4>.
- [243] M. Dong, O. Sahin, A nanomechanical interface to rapid single-molecule interactions, *Nat. Commun.* 2 (2011) 247, <https://doi.org/10.1038/ncomms1246>.
- [244] F. Rico, A. Russek, L. González, H. Grubmüller, S. Scheuring, Heterogeneous and rate-dependent streptavidin-biotin unbinding revealed by high-speed force spectroscopy and atomistic simulations, *Proc. Natl. Acad. Sci. U. S. A.* 116 (14) (2019) 6594–6601, <https://doi.org/10.1073/pnas.1816909116>.
- [245] M.R. Uhlig, C.A. Amo, R. García, Dynamics of breaking intermolecular bonds in high-speed force spectroscopy, *Nanoscale* 10 (2018) 17112–17116, <https://doi.org/10.1039/c8nr05715j>.
- [246] H. Yu, M.G.W. Siewny, D.T. Edwards, A.W. Sanders, T.T. Perkins, Hidden dynamics in the unfolding of individual bacteriorhodopsin proteins, *Science* 355 (6328) (2017) 945–950, <https://doi.org/10.1126/science.aah7124>.
- [247] H. Takahashi, F. Rico, C. Chipot, S. Scheuring, α -Helix unwinding as force buffer in spectrins, *ACS Nano* 12 (3) (2018) 2719–2727, <https://doi.org/10.1021/acsnano.7b08973>.
- [248] C. Marcuello, Current and future perspectives of atomic force microscopy to elicit the intrinsic properties of soft matter at the single molecule level, *AIMS Bioeng.* 9 (3) (2022) 293–306, <https://doi.org/10.3934/bioeng.2022020>.
- [249] J. Hou, N. Li, W. Zhang, W. Zhang, Exploring the impact of PEGylation on the cell-nanomicelle interactions by AFM-based single-molecule force spectroscopy and force tracing, *Acta Biomater.* 157 (2023) 310–320, <https://doi.org/10.1016/j.actbio.2022.12.020>.